Developments in the Built Environment 26 (2026) 100948

Contents lists available at ScienceDirect

Developments in the Built Environment

journal homepage: www.sciencedirect.com/journal/developments-in-the-built-environment

Influence of thermally activated industrial concrete fines of different origin on concrete long-term behavior

Jan P. Höffgen [a,*], Lukas Reichert [a], Bernd Susset [b], Annegret Walz [b], Peter Grathwohl [b], Frank Dehn [a]

[a] Karlsruhe Institute of Technology (KIT), Institute for Concrete Structures and Building Materials (IMB), Gotthard-Franz-Str. 3, Karlsruhe, 76131, Germany
[b] University of Tübingen, Department of Geosciences, Schnarrenbergstraße 94-96, Tübingen, 72076, Germany

ARTICLE INFO

Keywords:
Concrete
Cement
Mineral waste
Recycling
Thermal activation
Supplementary cementitious material

ABSTRACT

The use of thermally activated concrete fines as a supplementary cementitious material (SCM) offers a promising approach to construction-waste recycling. However, due to the lower reactivity of activated concrete fines compared to Portland cement, the substitution affects concrete performance, similar to established SCMs such as fly ash. While the composition of activated concrete fines varies, the effect on concrete compressive strength is similarly variable. The present study successfully adopts a previously developed model to compensate for compressive strength loss, which allows for the assessment of a wide range of concrete performance parameters for six different concrete fines. Results show that mechanical performance changes alongside compressive strength. The substitution of Portland cement negatively affects the resistance to carbonation, which is in-line with established SCMs. Chloride ingress lacks the positive effects of fly ash or slag. While concrete fines may contain harmful substances, elution results indicate parameter dependent effects of thermal activation.

1. Introduction

The use of inorganic wastes as supplementary cementitious materials (SCMs) offers an established approach to both resource efficiency and the reduction of CO_2-intensive Portland cement use.

When, during the concrete mixing process, Portland cement is partially substituted with SCMs, adjustments to the water-binder ratio are made to compensate for changes in compressive strength (Coffetti et al., 2022; Gao et al., 2013; Knight et al., 2023; Barthel et al., 2016). SCMs can be classified by their reactivity. Unlike Portland cement, most SCMs are non-hydraulic and rely on calcium hydroxide produced by Portland cement hydration to form calcium-silicate-hydrates. High-silicium SCMs, so-called pozzolans with calcium oxide to silicon dioxide molar ratios (C/S) lower than 0.5, consume calcium hydroxide (Barthel et al., 2016; Herrmann et al., 2018; Orozco et al., 2024). Latent-hydraulic SCMs with $0.5 < C/S < 1.5$ require calcium hydroxide as a catalyst for their hydration (Amran et al., 2021; Koenders et al., 2025). Both types of SCMs may provide additional reaction products, based on their individual chemical compositions (Snellings et al., 2023). In contrast, inert SCMs are nonreactive and serve as nuclei for cement hydration or as fillers that densify the cement paste (Scrivener et al., 2015; Panesar and Zhang, 2020).

However, the substitution also affects concrete long-term behavior, which is equally significant for the design of durable structures. Building standards rely on established empirical relationships to predict mechanical properties, long-term deformations, or corrosion resistance based on concrete compressive strength (International Federation for Structural Concrete, 2023). Cement substitution through pozzolanic or latent-hydraulic SCMs results in a reduction of early strength with a higher strength gain after 28 d (Nath and Sarker, 2011; Lübeck et al., 2012; Sakthivel et al., 2019). While the modulus of elasticity exhibits a similar behavior, total shrinkage is reduced, but increases for high substitution rates (Nath and Sarker, 2011; Darquennes et al., 2012; Sakthivel et al., 2019; Wang et al., 2022). Due to the reduced amount of $Ca(OH)_2$, the substitution of Portland cements leads to increased carbonation rates (Younsi et al., 2011; Gruyaert et al., 2013a,b). Chloride ingress is reduced due to the higher binding capacity of hydration products and a refinement of the pore system (Güneyisi and Gesoğlu, 2008; Nath and Sarker, 2011; Gruyaert et al., 2013a). The effect of inert SCMs strongly depends on their content, as the filler effect is only present for a low substitution rate. With increasing substitution, the dilution effect predominates, resulting in overall reduced concrete performance. However, for low substitution rates, the effect on strength and deformations is negligible (Wang et al., 2018).

* Corresponding author.
E-mail address: jan.hoeffgen@kit.edu (J.P. Höffgen).

https://doi.org/10.1016/j.dibe.2026.100948
Received 13 March 2026; Received in revised form 26 April 2026; Accepted 17 May 2026
Available online 25 May 2026

The search for additional SCMs has identified ground concrete fines as a promising precursor for Portland cement substitution (Aquino Rocha and Toledo Filho, 2023; Carriço et al., 2020a; Friol Guedes de Paiva et al., 2021; Kaliyavaradhan et al., 2020; Mao et al., 2024; Ohemeng and Ekolu, 2020; Pavlů, 2018; Rakhimova and Shi, 2024; Xu et al., 2022; Zheng et al., 2024). Those wastes consist of natural aggregates and hardened cement paste. Aggregates are mostly inert, but may exhibit a pozzolanic reactivity if they contain amorphous silicates (Lipowsky and Müller, 2017). Hardened cement paste can be thermally activated. At processing temperatures up to 700 °C, the different cement hydration products decompose and regain hydraulic reactivity (Angulo et al., 2022; Baggio et al., 2024; Baldusco et al., 2019; Baquerizo et al., 2016; Florea, 2014; Horváth et al., 1977; Klingsch, 2014; Schneider, 1982; Wang et al., 2019; Zelic et al., 2007; Zhou and Glasser, 2001; Zhou et al., 2004). Subsequently, mortar or concrete, where Portland cement is partially substituted by thermally activated concrete fines, exhibits the highest compressive strength in a range between 500 °C and 700 °C, with great variations between different publications (Bogas et al., 2019, 2022a; Chen et al., 2024; Kalinowska-Wichrowska et al., 2020; Sui et al., 2020; Tokareva et al., 2023; Wei et al., 2024; Wu et al., 2021; Xi et al., 2024; Zhang et al., 2022). Higher processing temperatures result in phase changes of dehydrated phases in addition to calcination of carbonatic phases (Klingsch, 2014; Noel et al., 2025; Real et al., 2020; Serpell and Lopez, 2015; Xu et al., 2023). Both processes are disadvantageous to producing high-strength cementitious materials (Noel et al., 2025; Real et al., 2020; Semugaza et al., 2023; Serpell and Lopez, 2015; Xu et al., 2023; Vyšvařil et al., 2014).

Similar to established SCMs, the Portland cement substitution using thermally activated concrete fines affects not only compressive strength but also short- and long-term mechanical and durability behavior. The aggregate fraction of concrete fines behaves as an inert SCM (Bogas et al., 2019; Carriço et al., 2021a,b). Dehydrated cement paste is porous, and during rehydration, these pores are filled by internal hydration products, mirroring the original porosity of the precursor (Bogas et al., 2020; Real et al., 2020; Semugaza et al., 2023; Vashistha et al., 2023; Wu et al., 2023; Xu et al., 2023; Xi et al., 2024). Cohesion between particles mainly stems from hydration products of primary cement, where the water consumption of cement paste locally reduces the water-binder ratio (Bogas et al., 2020; Serpell and Lopez, 2015; Baldusco et al., 2019).

Since the rehydration of dehydrated cement paste is a fast process, mortars containing thermally activated cement paste exhibit an accelerated strength development within the first days after mixing (Bogas et al., 2020; Real et al., 2020). Consequently, the compressive strength gain after 28 d is low (Bogas et al., 2020; Real et al., 2020; Kim and Kim, 2023; Semugaza et al., 2023). Overall, flexural strength development mirrors compressive strength (Bogas et al., 2020; Kim and Ubysz, 2024; Ma et al., 2022).

As activated concrete fines have a lower particle density compared to Portland cement, the partial substitution results in lower moduli of elasticity, even for low substitution rates, which do not affect compressive strength (Bogas et al., 2019; Real et al., 2021; Getachew et al., 2024).

The reduced particle stiffness also increases shrinkage deformations (Carriço et al., 2022; Real et al., 2021). Overall, increasing activation temperatures or concrete fines with low porosity result in decreasing shrinkage (Kim and Ubysz, 2024; Carriço et al., 2022; Tokareva and Waldmann, 2025). While the addition of activated concrete fines reduces basic shrinkage (Qian et al., 2020), drying shrinkage is sensitive to the amount of evaporable water, which results in increased deformations when high water-binder ratios are used for improving concrete workability (Kim and Ubysz, 2024; Carriço et al., 2022).

Capillary absorption strongly depends on porosity and pore structure, where increased water–cement ratios increase water uptake (Carriço et al., 2022). This trend is mitigated when water–cement ratios are held constant, allowing for a microstructural densification following water intake in activated cement paste particles (Bogas et al., 2022a; Carriço et al., 2022, 2021b). Increasing activation temperatures up to 1000 °C have a decreasing effect on capillary absorption (Kim and Ubysz, 2024; Ma et al., 2022; Wu et al., 2021, 2023; Tokareva and Waldmann, 2025). These observations also hold for freeze-thaw-damage (Algourdin et al., 2021; Wei et al., 2024).

As resistance to carbonation and chloride diffusion depends on porosity and the binding capacity of cement hydration products, increasing substitution rates have a negative impact (Bogas et al., 2022b; Carriço et al., 2021b; Xu et al., 2024). Chloride ingress reduces with increasing activation temperature and particle fineness (He et al., 2023; Kim and Kim, 2023; Qian et al., 2020).

These findings, with few exceptions (Algourdin et al., 2021; He et al., 2023; Wu et al., 2023; Tokareva and Waldmann, 2025), are based on artificial hardened paste or concrete as a precursor. However, industrial concrete fines from recycling plants never consist of pure paste, but contain varying amounts of aggregates with individual compositions. Besides, in contrast to artificial fines, industrial fines may contain harmful substances, such as organic components or heavy metals (Gao et al., 2015; Weimann, 2009; Wang et al., 2023; Van Praagh et al., 2015; Andrade et al., 2025). In the case of recycled concrete aggregates, heavy metals are mostly immobilized by cement hydration products and are, therefore, unsusceptible to leaching (Engelsen et al., 2010; Kurda et al., 2018; Lu et al., 2019). When cement hydration products are decomposed during an activation process, heavy metals regain solubility, but may be reabsorbed during a later reaction process (Park et al., 2025).

When using thermally activated concrete fines for substituting Portland cement in concrete applications, the overall influence on concrete strength, as well as deformations and long-term behavior, need to be accounted for. However, the available findings on concrete performance lack a broad dataset comprising fines of different compositions. With the application of established SCMs, negative effects on durability are usually mitigated by a reduction of the water-binder ratio alongside the compensation for strength reduction. This serves the goal of producing a concrete with a target strength, which follows the empirical relationships for relevant design properties. A novel model for assessing the impact of activated concrete fines on compressive strength was proposed by the authors of this study (Höffgen et al., 2025; Höffgen and Dehn, 2025). This allows for the design of concrete containing thermally activated fines with a target compressive strength. However, the effects on other concrete properties, beyond compressive strength, including the presence of harmful substances in concrete fines whose behavior may be altered by thermal activation, require additional consideration.

2. Experimental program

The experimental program, therefore, aims to assess the macroscopic properties of concrete incorporating thermally activated concrete fines from six different sources as supplementary cementitious material (SCM). These properties are compared with reference mixes incorporating established SCMs (granulated blast-furnace slag, coal fly ash, and limestone powder). Because compressive strength is the most important concrete property in structural design, the analysis is based on two different mixes from each SCM, each with a different strength. While one half of the mixes uses SCMs without accounting for their impact on compressive strength, the second half uses a model, previously published in Höffgen et al. (2025), to achieve a target compressive strength.

The experimental program follows the procedures of a previously published study by the authors, which focused on the effect of thermally activated artificial concrete fines with known compositions on concrete properties (Höffgen et al., 2026).

2.1. Materials

Six different concrete fines from five different recycling plants, labeled R1–R6, were selected based on preliminary analyses by the authors to account for a wide variation of material properties.

- R1: Fine fraction (<2 mm) from a recycled concrete aggregates production plant. The sample corresponds to A2-0/2 in Höffgen et al. (2025).
- R2: Fine fraction (<2 mm) from a recycled concrete aggregates production plant. The precursor contained grains with a diameter up to 8 mm, which were removed through manual sieving (F-0/2 in Höffgen et al. (2025)).
- R3: Ultrafine fraction (<250 μm) obtained by manually sieving R1 (A2-0/0.25 in Höffgen et al. (2025)).
- R4: Ultrafine fraction (<250 μm) similar to R3, but from a different recycling plant (B1-0/0.25 in Höffgen et al. (2025)).
- R5: Filter cake from a fresh concrete recycling plant (D–F in Höffgen et al. (2025)).
- R6: Filter cake from a crushed concrete recycling plant, which used a wet-separation process to remove hardened cement paste from recycled aggregates (G–F in Höffgen et al. (2025)).

During preprocessing, all materials were dried at 105 °C. The thermal activation used crucibles with a volume of 2.5 l, which were placed in a static furnace. Temperature was increased at a rate of 5 K/min until reaching the target temperature of 600 °C, which was held constant for 6 h. Passive cooling was performed in a container containing silica gel to maintain low relative humidity. Afterwards, activated concrete fines were stored in sealed buckets, except for the mechanical processing, where all concrete fines were milled until passing through a 125 μm-mesh. The activation procedure was adopted from previous investigations by the authors (Höffgen et al., 2025; Höffgen and Dehn, 2025).

Besides these six different activated concrete fines, concrete production used commercial Portland cement CEM I 42.5 R (according to EN 197-1:2011, labeled "CEM I") as base material, as well as ground granulated blast-furnace slag (EN 15167-1:2006, "S"), black coal fly ash (EN 450-1:2012, "FA"), and limestone powder (EN 12620:2008, "L") as reference SCMs with different reactivity. As aggregates, quartzitic river sand (0–2 mm) and fine gravel (2–8 mm) from the same source were used.

2.2. Experimental procedures

As the first step of the analyses, Portland cement (CEM I) and processed concrete fines were analyzed for their physical properties and chemical composition. Physical properties included particle size distribution (laser diffraction) and particle density (pycnometer). Nitrogen adsorption/desorption was used to determine both specific surface area (BET method) and porosity (BJH method). The chemical composition (in accordance with EN 196-2:2013) was determined by measuring the oxide phases of the main elements using wavelength-dispersive X-ray fluorescence (WDXRF) and the trace elements using energy-dispersive X-ray fluorescence (EDXRF) before activation. The analysis of reference SCMs (S, FA, L) comprised a reduced set of parameters. Additionally, activated concrete fines and CEM I were analyzed for their total and reactive CaO and SiO_2, as well as free CaO, the latter according to EN 451-1:2017. The chemical analyses were completed by the determination of sulfate (SO_3), carbon (C), and total organic carbon (TOC) through CSA (carbon–sulfur-analysis). CSA was also repeated on concrete fines prior to activation, with the additional determination of chloride content (Cl).

For *porosimetry* measurements, CEM I, reference SCMs, and activated concrete fines were used as binders to produce paste specimens with a water-binder ratio of $w/b = 0.5$. The share of SCMs of the total binder content was set to $f = 0.3$. Pastes with pure CEM I included $w/b = 0.6$ and $w/b = 0.5$, labeled CEM I-1 and CEM I-2. Pastes were mixed in a slurry mixer, filled in sealed plastic bottles, and placed in a specimen shaker to avoid segregation, before storage at 20 °C. At the age of 28 d, paste specimens were crushed with a chisel and sieved to a particle size between 2 mm and 4 mm for mercury intrusion porosimetry (MIP).

The concrete mix for the following analysis was designed with a paste content of $v_p = 40$ v%, a fine aggregates content of $v_s = 20$ v%, and a coarse aggregates content of $v_g = 40$ v%. For assessing the different kinds of SCMs, a fixed binder substitution rate of $f = 0.3$ by mass was chosen for all series. The water-binder ratio was set to $w/b = 0.5$ for the first series of mixtures. As all SCMs in this study were known to reduce compressive strength, a second series used a reduced water-binder ratio to produce concrete with similar compressive strength despite the substitution of CEM I. w/b was calculated for each SCM individually, based on estimated reactivity. This procedure relies on the k-value concept detailed in EN:206-2017 for reactive SCMs (see also Höffgen et al. (2025)). Table A.2 in the Appendix details the individual concrete mix designs, including estimates for k, and the resulting water-binder ratios and equivalent water–cement ratios. All series with a water-binder ratio of $w/b = 0.5$ were labeled with the suffix "−1", and series with an equivalent water–cement ratio of $w/c_{eq} = 0.5$ were labeled with the suffix "−2". Concrete without SCMs followed used a different naming scheme, where the mixture with $w/b = w/c_{eq} = 0.5$ used the suffix "−2". To allow for the assessment of varying strength, another concrete mix, CEM I-1 with an increased water-binder ratio of $w/b = w/c_{eq} = 0.6$ was produced.[1] Besides, CEM I-1 and CEM I-2 were partially repeated during the analysis to broaden the dataset. During mixing, PCE-based superplasticizer was added to ensure comparable workability.

For the experimental investigation of hardened concrete properties, from each mix 15 prisms ($(40 \times 40 \times 160)\,mm^3$) and one cylinder ($d = 100$ mm, $h = 280$ mm) were cast. Following demolding after 1 d, all specimens were stored at 20 °C under water, unless otherwise required by the testing procedures. Overall, for allowing the experimental investigation of various concrete properties with overlapping test schedules, simplified procedures were applied.

Strength testing used a total of six prisms, with the determination of the *flexural strength* ($f_{ct,fl}$) on three prisms each at the ages of 2 d and 28 d. These were immediately followed by *compressive strength* (f_c) measurements, but only on three prism halves each. The other halves were resubmerged in water for testing compressive strength at 56 d and 98 d. Testing followed the procedures in EN 196-1:2016.

Six prisms for the determination of the shrinkage development and the dynamic modulus of elasticity were stored in closed containers at 100 % r.h. rather than in water after demolding. Three prisms for *shrinkage* had cast-in measuring pins to measure specimen length with a dial gauge. Deformation measurements and specimen mass were recorded immediately after demolding and at the age of 7 d (t_0). Afterwards, the specimens were stored in a climate chamber at 65 % r.h. Subsequent measurements were performed at the age of 14 d, 21 d, 35 d, 63 d, and 98 d. Resulting deformations were normalized to the prism length, yielding the shrinkage strain over time ($\varepsilon_{cs}(t)$). Prisms for the *dynamic modulus of elasticity* (E_c) were stored alongside shrinkage specimens until ultrasonic pulse measurements at the age of 28 d. Afterwards, these prisms were tested for their flexural and compressive strength at the ages of 28 d and 98 d, respectively.

The three remaining prisms were removed from the water storage at the age of 28 d and placed in a climate chamber at 65 % r.h. for 14 d. Afterwards, specimens were moved to a *carbonation* chamber with

[1] CEM I-1 and CEM I-2 are identical to reference mixes in a previous study by the authors (Höffgen et al., 2026). All other concrete mixes, and subsequent results, are unique to this study.

Table 1
Results of the physical and wet-chemical analysis of CEM I, reference SCMs (S, FA, L) and concrete fines (R1–R6) before activation ("−100") and after activation at 600 °C ("−600").
ρ_ρ: particle density, S_{BET}: specific surface area, p_{BJH}: pore volume, d_{10}, d_{50}, d_{90}: particle size at 10 v%, 50 v%, and 90 v% cumulatively passing, C: Carbon, TOC: total organic carbon, Cl: chloride, S: sulfur, SO_3: sulfate, (f/r-)CaO: total, free, and reactive calcium oxide, (r-)SiO_2: total and reactive silicon dioxide.

	ρ_ρ $\frac{kg}{dm^3}$	S_{BET} $\frac{m^2}{g}$	p_{BJH} $\frac{cm^3}{kg}$	d_{10} µm	d_{50} µm	d_{90} µm	C wt%	TOC wt%	Cl wt%	S wt%	SO_3 wt%	CaO wt%	f-CaO wt%	r-CaO wt%	SiO_2 wt%	r-SiO_2 wt%
CEM I	3.13	1.4	7.1	1.7	12.1	32.9	0.5	0.01	0.07	1.22	3.0	61.7	0.77	57.7	20.4	19.5
S	2.92	0.9	3.9	2.1	12.3	30.0										
FA	2.25	7.6	14.0	2.9	21.6	83.4										
L	2.70	5.7	14.4	1.9	12.5	44.4										
R1-600	2.65	4.8	28.2	1.9	17.9	88.4	3.2	0.03		0.28	0.7	22.1	0.04	8.1	54.3	8.8
R2-600	2.64	3.3	21.9	2.3	25.9	99.1	1.5	0.02		0.17	0.4	12.2	0.04	8.2	71.2	8.4
R3-600	2.64	5.9	34.0	1.8	14.1	81.0	3.2	0.03		0.35	0.9	22.8	0.06	8.8	52.2	10.1
R4-600	2.60	6.8	41.1	2.0	18.4	97.6	2.5	0.02		0.45	1.1	21.4	0.10	10.8	54.5	13.3
R5-600	2.64	13.6	87.3	2.0	18.8	96.2	1.5	0.03		0.44	1.0	23.8	0.17	17.2	56.6	13.7
R6-600	2.66	12.8	72.3	1.8	11.6	40.5	3.0	0.07		0.37	0.9	19.8	0.05	7.7	47.0	14.5
R1-100							3.5	0.15	0.04	0.27						
R2-100							1.7	0.12	0.01	0.19						
R3-100							3.7	0.24	0.04	0.39						
R4-100							3.0	0.35	0.01	0.45						
R5-100							2.1	0.18	0.04	0.50						
R6-100							4.1	0.99	0.04	0.37						

57 % r.h. and 3 v% CO_2. After exposure for 7 d, 28 d, and 70 d, the prisms were temporarily removed from the carbonation chamber and split, to produce a fresh surface for measuring the carbonation depth with the phenolphtalein indicator test on three measuring points per edge. The accelerated carbonation coefficient (K_{AC}) was then calculated as the slope of the development of the mean carbonation depth over the square root of exposure duration according to EN 12390-12:2020.

Water storage of the cylinder was shortly interrupted when the specimen was cut into five smaller slices with a height of approximately 45 mm. These were then sealed with an epoxy resin, baring both flat surfaces of two cylinder slices and one flat surface of each of the three remaining slices. All specimens then reentered water storage until the age of 28 d. The specimens with one unsealed flat surface were conditioned in a saturated $Ca(OH)_2$-solution for 24 h before storage in a 16.5 wt%-NaCl-solution. After 35 d, specimens were split, and the *chloride* penetration depth (d_c) was determined using the silver nitrate indicator test as an average of nine datapoints per specimen half. While this procedure is usually applied for evaluating the rapid chloride migration test (i.e., EN 12390-18:2021), the time-consuming determination of chloride profiles, which allows for the calculation of the chloride diffusion coefficient (D_{nss}) according to EN 12390-11:2015, was only performed for two additional specimens of the concrete mix CEM I-2.1.

The remaining two cylinder slices with sealed lateral surfaces were stored at 65 % r.h. for at least 6 months until reaching constant weight. The *capillary absorption* coefficient $WA_{24\,h}$ was determined by normalizing the mass change after partially (5 mm) submerging the cylinders in water for 24 h, to the surface area.

The *leaching* behavior of concrete fines was investigated in a three-step approach, using the percolation method specified in German standard DIN 19528:2023-07. The first and second steps used concrete fines before and after thermal activation, without grinding. For the third step, concrete prisms for strength testing from the "−1" series were dried at 105 °C and crushed to a maximum particle size of 4 mm. The materials were compacted in columns, with steps 1 and 3 using a target volume of $v_c \approx 500$ ml and step 2, for material availability reasons, limited to $v_c \approx 90$ ml. The water-solid ratio was set to $w/s = 2$ for all tests. The eluates were evaluated for their anion (ion chromatography), metal (inductively coupled plasma mass spectrometry), and PAH (Polycyclic Aromatic Hydrocarbons, gas chromatography-mass spectroscopy) fractions.

3. Results and discussion

3.1. Characterization of binders

Table 1 details the physical and chemical characterization of CEM I, reference SCMs (slag, fly ash, and limestone powder), as well as processed concrete fines.

The physical properties of slag are similar to CEM I. Limestone powder exhibits a slightly higher maximum particle size with higher specific surface area and pore volume. Among the reference SCMs in this study, fly ash exhibits the coarsest particle-size distribution, the lowest density, and the highest specific surface area and pore volume.

On average, activated concrete fines exhibit a similar specific surface area and particle size distribution as fly ash, albeit at a higher particle density and higher pore volume. Individually, specific surface area and pore volume depend on the preprocessing procedure, with smaller particles prior to activation yielding higher values. This is not reflected in the particle size distribution. R1-600 and R3-600, from the same processing plant, have higher concentrations of fine particles than the other samples. The only exception is R6-600, which has a significantly lower d_{90}, suggesting a smaller filter size than R5-600. Since particle size and specific surface area are independent, a remaining explanation is the hypothesized concentration of hardened cement paste particles with reduced precursor particle size (Juan and Gutiérrez, 2009). This also corroborates the observed increase in specific surface area and porosity with smaller precursor particle size, since dehydrated cement paste exhibits a loose microstructure with high porosity (Baldusco et al., 2019; Bogas et al., 2019; Carriço et al., 2020b; Kim et al., 2021).

Table A.3 in the Appendix section details the chemical composition of CEM I, reference binders, and concrete fines before activation. CEM I consists of CaO, SiO_2 and, to a lesser amount, Al_2O_3 and Fe_2O_3, which corresponds to a typical Portland cement composition (Andrade Neto et al., 2025). Slag and fly ash exhibit an increased share of both SiO_2 and Al_2O_3, while CaO decreases. Limestone powder, on the other hand, almost exclusively consists of CaO (in the form of $CaCO_3$, as indicated by the high loss on ignition). The chemical composition of concrete fines varies, with generally high amounts of SiO_2 and CaO. In general, the comparison of results across the three preprocessing groups reveals that the smaller precursor particle size of R3/R4 is associated with a higher CaO to SiO_2 ratio, and this trend becomes even more pronounced for R5/R6. However, because both CaO and SiO_2 are

present in aggregates and in hydrated cement paste, WDXRF results are not suitable for assessing the reactivity of concrete fines. Table 1 details results of the wet-chemical analyses for CEM I and activated concrete fines. The increase of CaO and SiO_2, compared to WDXRF, can be explained through the mass loss during activation. In contrast to WDXRF, the wet-chemical analysis enables the determination of reactive CaO and SiO_2. In CEM I, most of CaO and SiO_2 are reactive, with only minor inert components, presently in the form of carbonates or sulfates. In activated concrete fines SiO_2 and, to a lesser extent, CaO are mostly inert. Reactive SiO_2 increases with higher precursor fineness. Reactive CaO shows a similar trend, except for R6. Consequently, the reactive CaO/SiO_2 molar ratio ranges between 0.6 for R6 and 1.3 for R5. The amount of free CaO, which includes $Ca(OH)_2$, is particularly low for all activated concrete fines, which suggests an extended carbonation of all precursors.

3.2. Porosity

The partial substitution of CEM I through SCMs affects the pore radius distribution (see Fig. 1). For all SCMs tested at a constant water-binder ratio, this is reflected in a shift in gel porosity with pores smaller than 50 nm. In contrast, an increased water–cement ratio also increases capillary porosity in the range of 100 nm–1000 nm.

Limestone powder (L) has the most significant effect on porosity, while slag (S) only marginally affects the pore size distribution, compared to CEM I at the same water-binder ratio. The impact of activated concrete fines is similar to fly ash (FA), which shows a minor shift of the gel porosity and a slight increase of capillary porosity (compare Vashistha et al., 2023; Wu et al., 2021; Wei et al., 2025). Overall, the activated fines exhibit a similar pore-radius distribution regardless of preprocessing.

3.3. Compressive strength development

The results from compressive strength measurements, as shown in Fig. 2, exhibit the hypothesized behavior. Compressive strength at 28 d of concrete mixes with a constant (equivalent) water–cement ratio of 0.5 ("−2") is similar for all series, while mixes with a constant water-binder ratio, and subsequently increased (equivalent) water–cement ratios ("−1") have a reduced compressive strength.

For concrete containing activated fines, compressive strength increases with reduced precursor particle size. This confirms the applied k-values for the individual SCMs and activated fines, except for R5-600, where the increased compressive strength of both mixes suggests a higher k-value. The high strength for R5-600 aligns with the highest share of reactive CaO and SiO_2 (see Table 1 and Fig. 3). A similar effect of reactive CaO is also apparent, but less pronounced. Furthermore, R5-600 paste exhibits the lowest porosity of all pastes measured. However, the general relationship between porosity and compressive strength is relatively weak compared with CEM I and reference SCMs (see Fig. 3), thereby corroborating the results in Xi et al. (2024).

The illustration of porosity and compressive strength in Fig. 3 uses the reference strength $f_{c,ref}$, which results from the assessment of the temporal strength development. Here, the empirical model from *fib* Model Code 2020 (International Federation for Structural Concrete, 2023) in Eq. (1) was fitted to the experimental data from each concrete series by applying the least squares method. Subsequently, $f_{cm,ref}$ denotes the compressive strength at the reference age (t_{ref} = 28 d). $f_{cm,ref}$ was obtained as a result from the fit, rather than used as an input parameter, to obtain a stabilized reference strength for later comparisons. For most series, $f_{cm,ref}$ is similar to $f_{c,28\,d}$, but some series show larger deviations, which may be subject to random influences during storage and testing. Most noteworthy is FA-2, for which the double determination yields substantial differences at the testing ages 56 d and 98 d. The other repeated series (CEM I-1 and -2 as well as FA-1) show a good reproducibility.

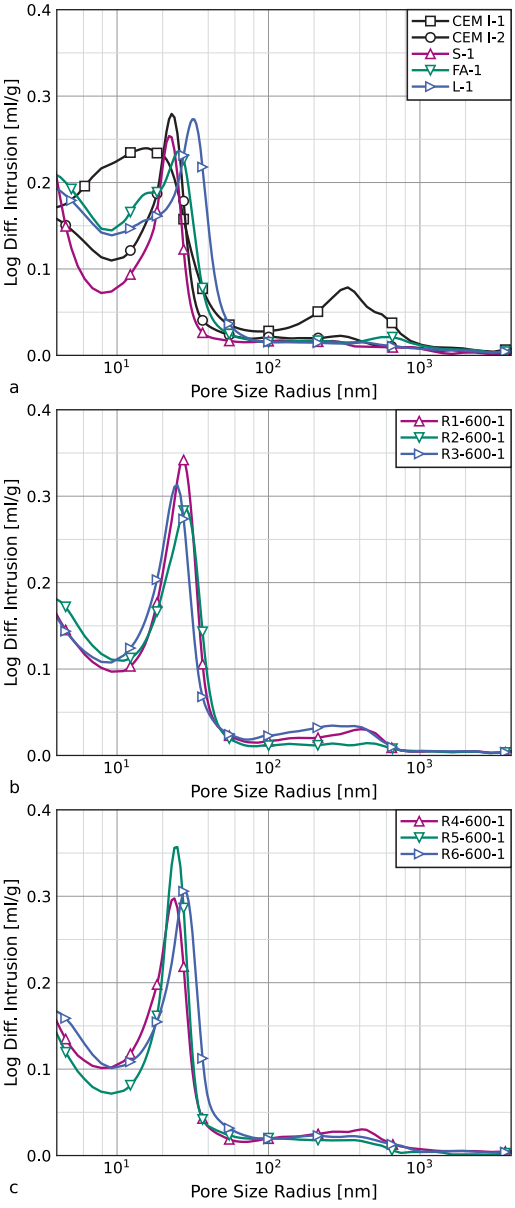

Fig. 1. Differential pore radius distribution (logarithmic) for reference series CEM I-1 and CEM I-2 and established SCMs S, FA, and L (a), as well as thermally activated concrete fines from (b and c).

$$f_c(t) = f_{cm,ref} \cdot \exp\left\{ s_c \cdot \left[1 - \left(\frac{t_{ref}}{t} \right)^{0.5} \right] \right\} \quad (1)$$

The second parameter in Eq. (1), s_c, describes the velocity of the strength development, with lower values indicating high early strength, and high values signifying increased strength gain after the reference age t_{ref}. In *fib* Model Code 2020 (International Federation for Structural Concrete, 2023), s_c ranges between 0.2 for concrete with cement strength class CR and 35 MPa < f_{ck} < 60 MPa, and 0.3 for $f_{ck} \leq$ 35 MPa.[2] For strength class CN, these values increase to 0.4 and 0.5, respectively. Presently, concrete mixes "CEM I" can be classified as

[2] *fib* Model Code 2020 (International Federation for Structural Concrete, 2023) defines f_{ck} as the characteristic cylinder compressive strength. To enable a comparison with present data, $f_{cm,ref} \approx f_{ck}$ + 18 MPa can be assumed. The offset comprises the difference between the mean and characteristic

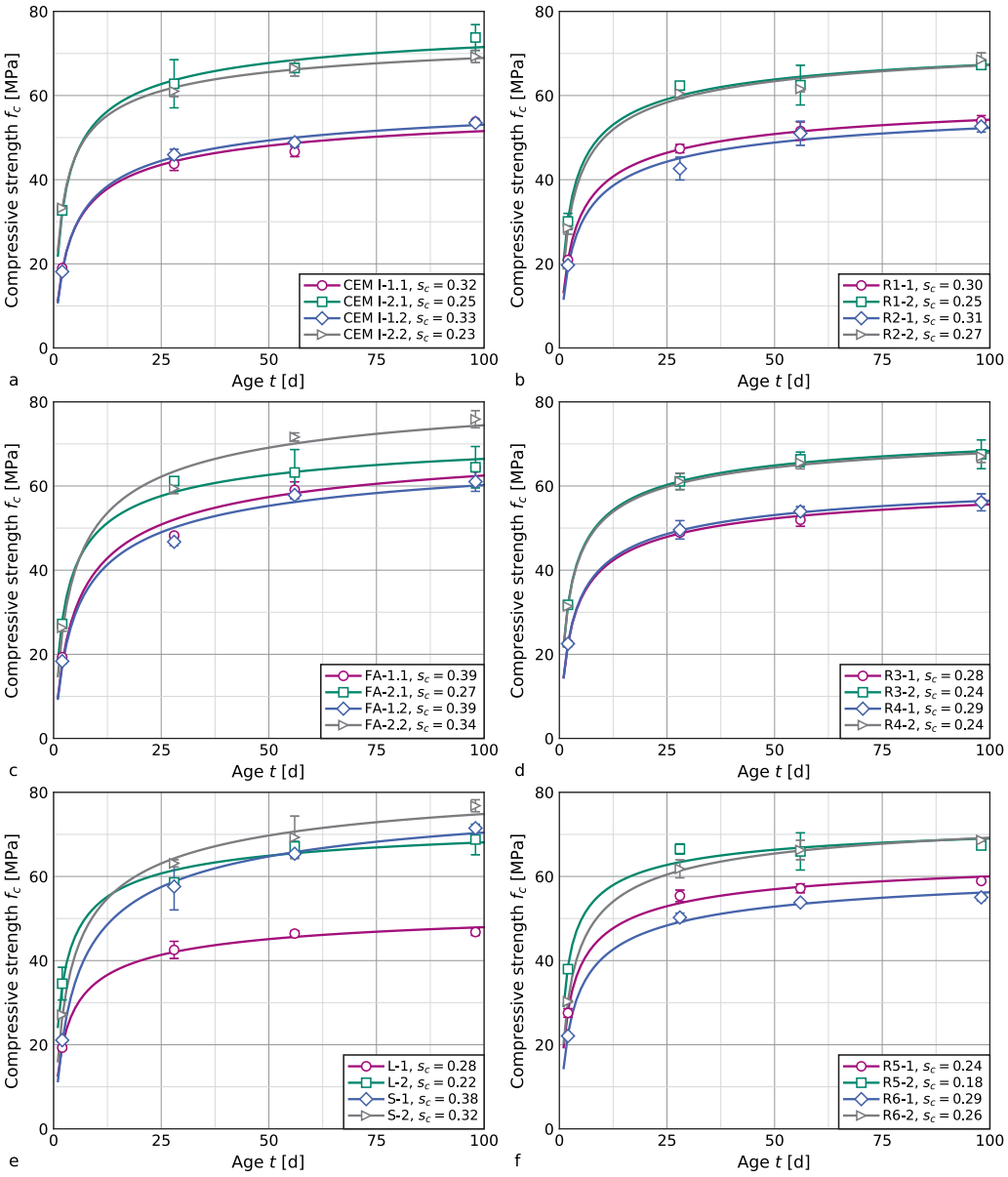

Fig. 2. Temporal development of compressive strength for reference mixes (a, c, d), and concrete containing activated fines (b, d, f). Diagrams for CEM I and FA show results from repeated concrete mixes. Markers indicate the measured averages and standard deviations from three prisms; lines represent the corresponding fit curves used to determine $f_{cm,ref}$ and s_c (Eq. (1)).

strength class CR, and concrete mixes "FA" match the description of strength class CN. Present results for CEM I fit these provisions, as illustrated in Fig. 4. s_c for the four series "FA" tend to fall below the provisions in International Federation for Structural Concrete (2023), indicating a faster-than-expected strength development. Findings for concrete incorporating slag are similar to those for fly ash, whereas limestone powder has a marginally accelerating effect on the temporal development of strength. All concrete series with activated concrete fines exhibit s_c in the range of CEM I for the entire compressive strength range, which signifies a fast compressive strength development similar to CEM I.

An alternative, simplified method for assessing compressive strength development is the quotient r in Eq. (2), which is, however, limited to strength results at 2 d and 28 d.

$$r = \frac{f_{c,2\,\mathrm{d}}}{f_{c,28\,\mathrm{d}}} \tag{2}$$

Fig. 4 shows the results for both evaluation methods. Except for FA-2, all concrete mixes with slag or fly ash yield the highest values of s_c and the lowest values of r. Concrete mixes with activated concrete fines exhibit similar results as the CEM I base mixes or the reference series, where limestone powder partially replaces CEM I (compare Bogas et al., 2020; Real et al., 2020; Kim and Kim, 2023; Semugaza et al., 2023).

3.4. Flexural strength

A benefit of using prisms for strength testing, according to EN 196-1:2016, is the ability to measure flexural strength alongside compressive strength on the identical specimens. In the present study, flexural strength was determined on three water-cured specimens at the ages of 2 d and 28 d and on dry-cured specimens at the ages of 28 d and 98 d.

compressive strength of 8 MPa and the difference between the cubic and cylindrical compressive strength of 10 MPa.

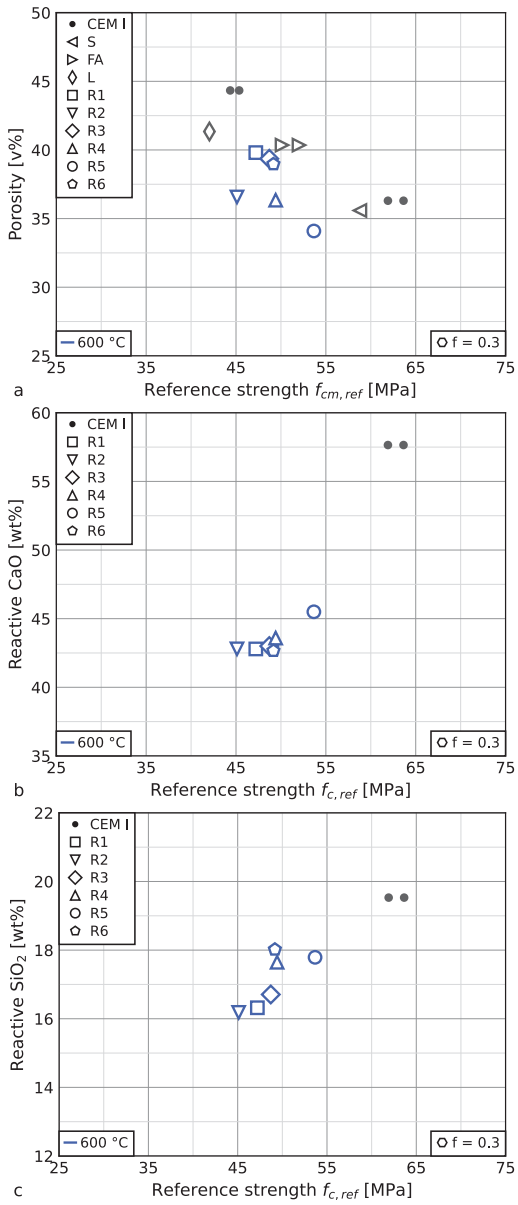

Fig. 3. Relationship between concrete compressive strength $f_{cm,ref}$ and total paste porosity (a), total reactive CaO (b) and total reactive SiO_2, both as the weighted sum of CEM I and R1-R6.

Fig. 5 illustrates the results of flexural and compressive strength tests of water-cured prisms.

The relationship between flexural and compressive strength follows a nonlinear trend (compare Campos et al., 2021; Liu et al., 2023; International Federation for Structural Concrete, 2023), with overall minor deviations. Furthermore, these deviations are independent of testing age and cement substitution with SCMs or activated concrete fines. Overall, the only influencing factor on flexural strength appears to be compressive strength, suggesting good transferability of design specifications for established SCMs to thermally activated concrete fines.

3.5. Dynamic modulus of elasticity

The dynamic modulus of elasticity was determined in this study as an inexpensive and rapid alternative to measuring the static modulus of elasticity. Nonetheless, the results obtained from ultrasonic pulse measurements allow for the qualitative assessment of the impact of activated concrete fines on the modulus of elasticity, because the overall concrete composition and the curing conditions were not varied throughout the test series (Ekin and Uyanik, 2021; Marques et al., 2020).

Fig. 6 compares results of the experimental determination of the dynamic modulus of elasticity to the prism compressive strength, which were determined on the identical specimens at the age of 28 d.

In addition to the increase in the dynamic modulus of elasticity with increasing concrete compressive strength, which corroborates findings in Getachew et al. (2024), the results indicate an effect of cement substitution with SCMs. While slag and limestone powder exhibit results similar to those of the base mixes with CEM I, the substitution with fly ash tends to increase the dynamic modulus of elasticity. Although compressive strength remains the most significant factor affecting the dynamic modulus, the present results show a decrease in the dynamic modulus with increasing reactivity of activated concrete fines, regardless of compressive strength. R1-600 and R2-600, which exhibit the lowest reactivity, have higher dynamic moduli than the base and reference mixes. The lowest dynamic moduli are achieved by R5-600, which shows the highest reactivity among all concrete mixes.

The reason for this may lie within the high porosity of dehydrated cement paste, and, subsequently, of thermally activated concrete fines with increasing paste content (compare Table 1). In contrast to established reactive SCMs like fly ash or slag, hydration products in activated concrete fines tend to form inside the porous particles, so that rehydrated fines exhibit a similar porosity as the respective precursors and no overall paste densification (Bogas et al., 2019; Real et al., 2021). On the other hand, a high content of inert aggregate particles within activated fines acts similarly to limestone powder and increases material stiffness (compare Wang et al., 2018).

3.6. Shrinkage

Concrete shrinkage comprises various components, with drying shrinkage being the primary factor. This type of shrinkage results from the loss of evaporable water (International Federation for Structural Concrete, 2023). In the case of normal-strength concrete, shrinkage caused by cement hydration is relatively minor and can be overlooked (Müller et al., 2021). To eliminate the impact of this type of shrinkage on the measured deformations, the specimens were kept at 100 % r.h. until they were 7 d old.

The development of shrinkage deformations over time, up to 98 d of concrete age, is illustrated in Fig. 7. Given that the difference in deformations between 1 d and 7 d of age is inconsistent and smaller than the standard deviation of the measurements, it is logical to disregard basic shrinkage. As a result, the shrinkage deformation ε_{cs} observed from 7 d of age onward is attributable solely to drying shrinkage.

Evaluating shrinkage deformations can be challenging due to high data variability, particularly when measurements are taken intermittently. To address this, the material model proposed in International Federation for Structural Concrete (2023) was employed to enhance the analytical framework. This model incorporates a drying shrinkage coefficient, a humidity coefficient, and a time function. Since humidity remains constant in this study, Eq. (3) simplifies this approach to include only the time function and the shrinkage coefficient ε_{cs0}, representing the ultimate shrinkage deformation.

$$\varepsilon_{cds}(t,t_s) = -\varepsilon_{cs0} \cdot \left(\frac{t - t_s}{0.035 \cdot h^2 + (t - t_s)} \right)^{0.5} \tag{3}$$

For all concrete mixes, Eq. (3) was fitted to the evolution of the mean shrinkage deformations over time. As the parameter h in Eq. (1) represents specimen geometry, which was identical for all specimens, the parameter ε_{cs0}, resulting from the least-squares method, describes the summarized influence of the cement substitution through SCMs and activated concrete fines.

While International Federation for Structural Concrete (2023) includes an increase in shrinkage deformation with decreasing compressive strength, this effect only shows for the individual types of SCMs

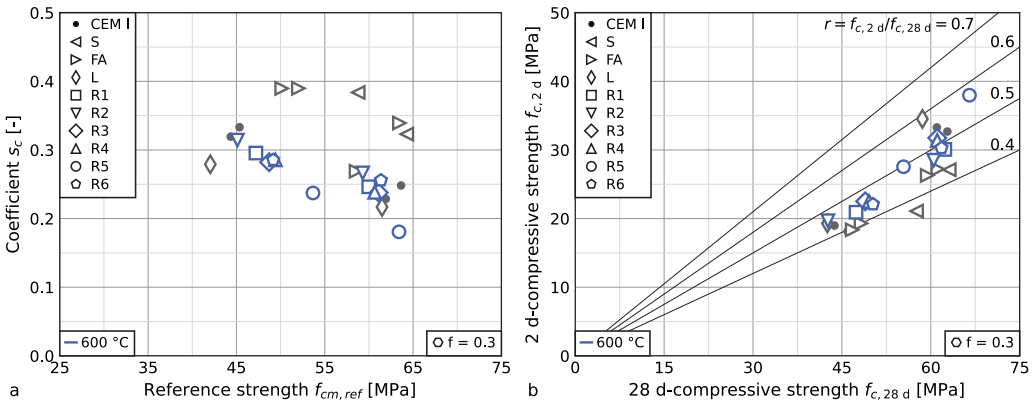

Fig. 4. Temporal development of compressive strength. Relationship between parameters $f_{cm,ref}$ and s_c from fitting Eq. (1) to experimental results after 2 d, 28 d, 56 d and 98 d (a) and relationship between experimental compressive strength at 2 d and 28 d (b).

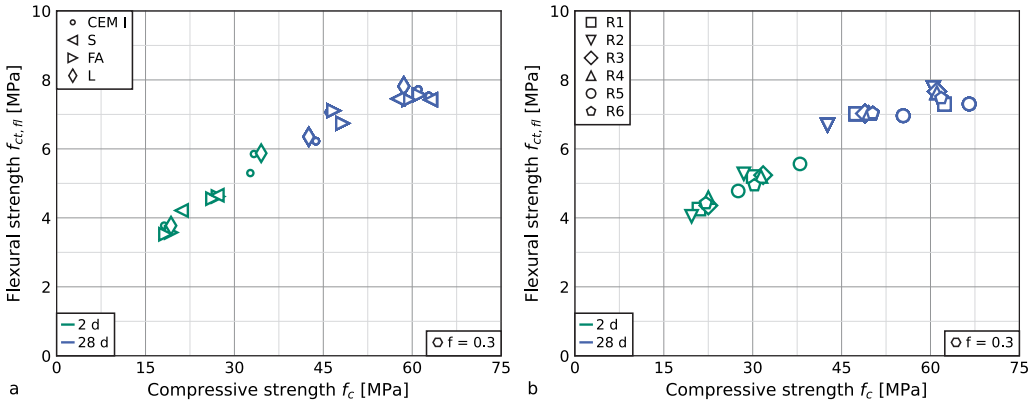

Fig. 5. Relationship between flexural and compressive strength at 2 d and 28 d after water-storage. Reference mixes with CEM I, S, FA, and L (a), and concrete mixes containing activated concrete fines (b).

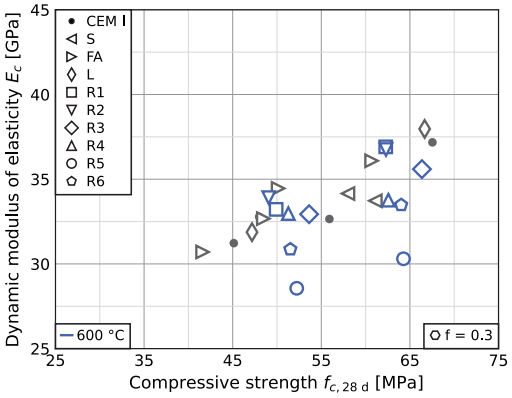

Fig. 6. Relationship between compressive strength and dynamic modulus of elasticity at the age of 28 d.

and activated concrete fines: For all mixes within this study, the "−1"-series with lower strength exhibits higher shrinkage deformations (see Fig. 8). However, the variation among these series is significantly greater than the effect of compressive strength. Nonetheless, it is evident that activated concrete fines, as well as slag, increase shrinkage, whereas fly ash and limestone powder have a decreasing effect (Nath and Sarker, 2011; Sakthivel et al., 2019; Darquennes et al., 2012; Wang et al., 2022). The scatter reduces when, instead of $f_{cm,ref}$, the dynamic modulus of elasticity is used as the base parameter. This suggests similar influencing factors, such as the mitigating effect of a high amount of inert particles, which hinder shrinkage due to their high stiffness. At the same time, a high amount of reactive phases, such as those present in R5-600, allows for higher deformation, as shrinkage only occurs in the cement paste.

3.7. Capillary absorption

The capillary water absorption coefficient $WA_{24\,h}$ for concrete containing thermally activated concrete fines increases with decreasing strength with minor deviations from the trendline. An identical pattern is observed for concrete containing limestone powder, with series L-1 exhibiting the lowest compressive strength and the highest water absorption among all series in this study. However, while the compensation of compressive strength loss due to partial cement replacement through the effective water–cement ratio also negates any measurable effects on water absorption, series CEM I-1 exhibits a reduced water absorption coefficient at a compressive strength similar to R1-600 and R2-600. This effect can, to a lesser extent, be observed for the cement substitution through slag or fly ash. Fig. 9(a) illustrates these findings.

These observations do not align with the results for total porosity, in contrast to the findings in Wu et al. (2023) on the influence of the substitution rate. However, the influence of compressive strength confirms previous findings on activated artificial cement paste (Bogas et al., 2022a; Carriço et al., 2022, 2021b). The overall increase in water absorption alongside a decrease in compressive strength is consistent with previous findings in Kim and Ubysz (2024), Bogas et al. (2022b) and Wu et al. (2023).

3.8. Chloride diffusion

The determination of the chloride profiles from profile grinding of series CEM I-2.1 yielded a diffusion coefficient of $D_{nss} = 296\,mm^2/a =$

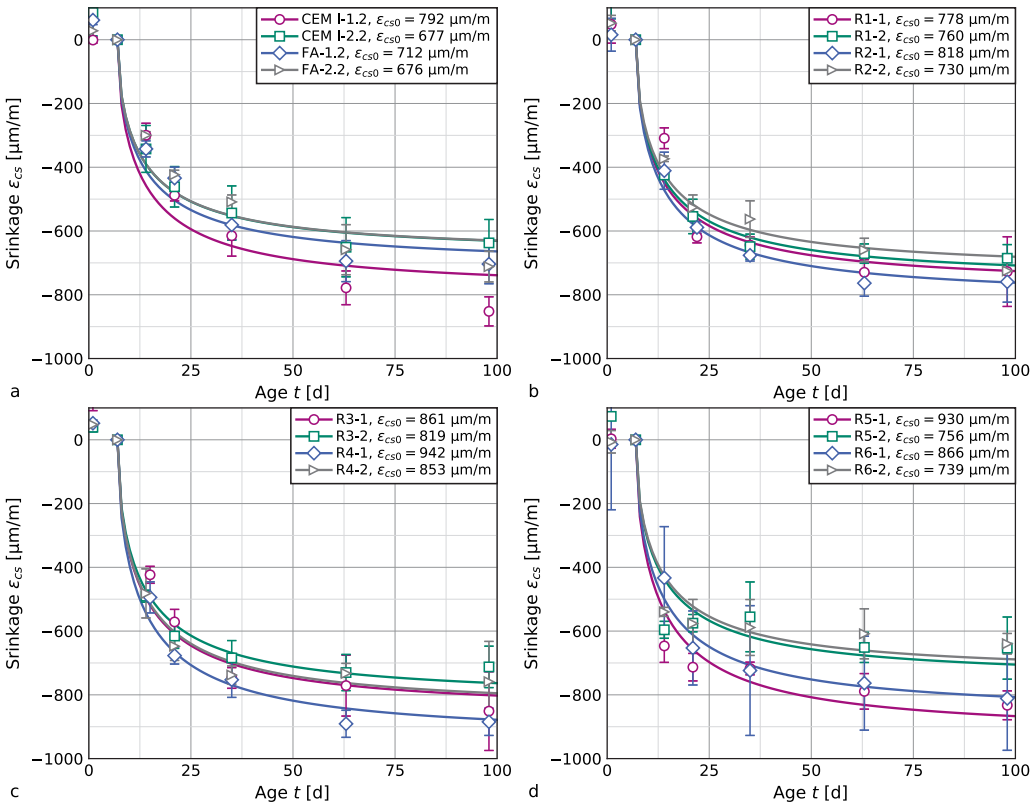

Fig. 7. Temporal development of shrinkage deformation for reference mixes (CEM I-1.2, CEM I-2.2, FA-1.2, FA-2.2, a), and concrete containing activated fines (b–d). Markers indicate the measured averages and standard deviations from three prisms; lines represent the corresponding fit curves used to determine ε_{cs0} (Eq. (3)).

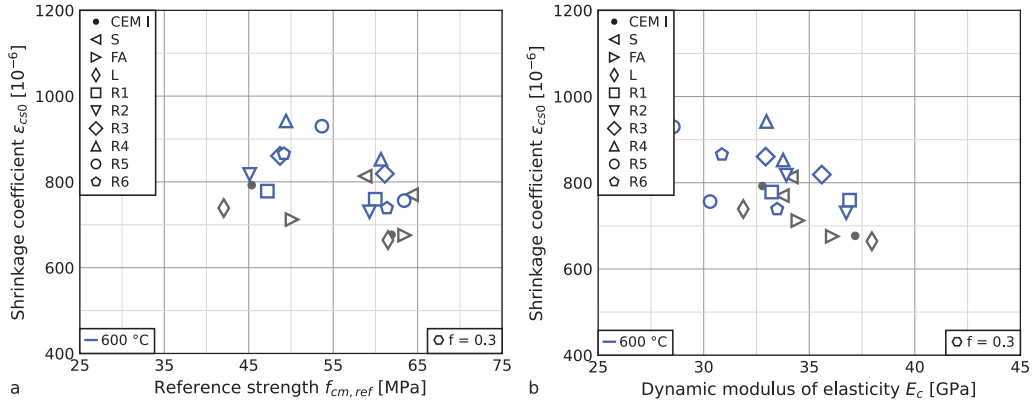

Fig. 8. Relationship between shrinkage coefficients ε_{cs0} and reference compressive strength $f_{cm,ref}$ (a), or dynamic moduli of elasticity E_c (b).

$9.4 \times 10^{-12}\,\mathrm{m^2/s}$ and a superficial chloride content of $C_s = 1.14\,\mathrm{wt\%}$ with an initial chloride content of $C_i = 0.02\,\mathrm{wt\%}$, both relative to the mass of concrete. The average chloride penetration depth of $d_c = 8.8\,\mathrm{mm}$, obtained from the silver nitrate indicator test on specimens from the same series, corresponds to a chloride content of $C = 0.28\,\mathrm{wt\%}$ normalized to the mass of concrete.

The silver nitrate indicator test on specimens from the repetition of this series yielded a penetration depth of $d_c = 12.6\,\mathrm{mm}$. The repeated series CEM I-1, FA-1, and FA-2 show a similar offset between the measurements (compare Fig. 9b). As the respective specimens were produced at the beginning and at the end of the study, which spanned several months, an inhomogeneity in the chloride content of the raw materials cannot be ruled out by the interpretation. However, the results show increased chloride penetration depth in concrete mixes containing activated concrete fines compared with the reference series containing pure CEM I, slag, or fly ash. An increased chloride content of concrete fines can be ruled out as a cause due to the results presented in Table 1. An alternative explanation is the chloride-binding capacity of hydration products from CEM I, slag, and fly ash, which is apparently absent in activated concrete fines (compare Liu et al., 2023). This agrees with previous findings, which identified a temperature dependence of the chloride-binding capacity of thermally activated concrete fines (He et al., 2023; Carriço et al., 2021b).

3.9. Carbonation

The results in Fig. 9(c) show a similar behavior of concrete containing activated fines on carbonation as on chloride ingress. However, activated concrete fines have a lower carbonation coefficient K_{AC} than

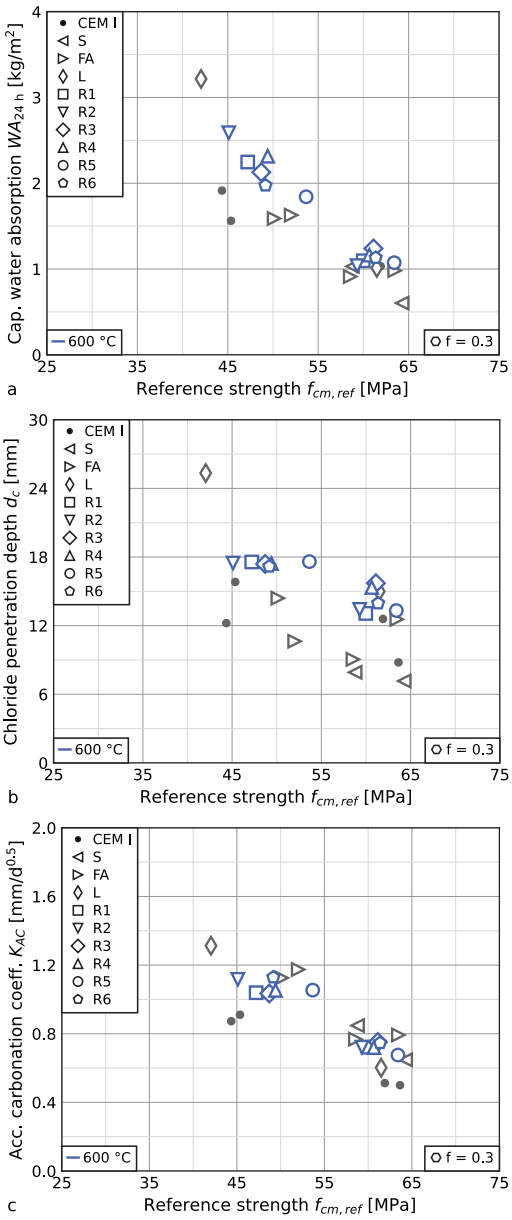

Fig. 9. Influence of compressive strength on concrete durability: Capillary water absorption (a), chloride penetration depth (b), and accelerated carbonation coefficient (c).

mixtures containing fly ash, and are similar to limestone powder and slag. A reason for this behavior may lie in the reduced alkalinity of the pore solution, which stems from $Ca(OH)_2$ forms during the hydration of CEM I. While limestone powder or slag reduces the $Ca(OH)_2$-content through the reduction of CEM I, the pozzolanic reaction of fly ash consumes $Ca(OH)_2$ and subsequently lowers the binding capacity of CO_2. The renewed formation of calcium-silicate-hydrates from dehydrated paste does not require additional $Ca(OH)_2$. Simultaneously, results in Table 1 show a negligible amount of free CaO, which implies a similarity to the reaction of slag. These findings confirm and expand on previously published results (Carriço et al., 2021b; Bogas et al., 2022b).

3.10. Leaching

Fig. 10 illustrates findings for select trace metal contents and organic compounds determined through both EDXRF and selected percolation tests. Tabulated results are depicted in Tables A.3, A.4, A.5, and A.6 in the Appendix.

Metal content in concrete fines varies widely. While EDXRF yields concentrations near or below the detection limit, some metals, exemplified in Fig. 10a, exhibit elevated concentrations, albeit with substantial differences among them. Overall, but not universally, metal concentrations increase with higher precursor fineness. Among the established SCMs, slag and limestone exhibit metal concentrations lower than those of most RCFs, whereas fly ash shows the highest concentrations of all materials. Results agree with findings listed in Park et al. (2025).

Percolation tests were performed to determine which of these metals are prone to leaching by water and therefore pose a potential risk of environmental contamination. Due to the high labor- and time intensiveness of this method, percolation for a water/solid ratio of $w/s = 2$ was limited to unaltered concrete fines, thermally activated fines, and concrete mixes containing activated fines with a constant water-binder ratio of $w/b = 0.5$. Results in Fig. 10b indicate a distinct variation between different metals, with Cr and Cu showing a higher elution compared to the other metals. On average, the eluates contain 0.34(30) % of the total Cu and 0.16(12) % of the total Cr content. For Ni, the ratio is 0.08(6) %, and 0.03 % or lower for other metals.

Yet, the behavior is strongly affected by the thermal activation (Fig. 10c). The eluble content of As, Cu, Ni, and Pb reduces, while Zn remains unaffected. A possible explanation for this behavior might lie in the immobilization of metals in dehydrated cement paste particles. Cr, however, behaves contrarily, with a significantly increased elution for thermally activated concrete fines. This may be triggered by the oxidation of Cr(III) to Cr(IV) at temperatures higher than 200 °C (Wang et al., 2025). While it is established that Cr, like other metals, can be immobilized in cement hydrates, this immobilization apparently fails upon decomposing the hydrates. This corroborates findings in Ma et al. (2023), where the leaching of Cr in acidic solutions increases with processing temperatures up to 800 °C. However, in contrast to the present study, this effect is also reported for other metals Ni, Cu or Pb, while Zn exhibits a decreasing behavior, albeit with a strong influence of the leaching solution (Ma et al., 2023).

Regardless, the elution of crushed concrete containing activated fines (Fig. 10d) exhibits a very similar behavior, and especially in the case of Cr, an apparent renewed immobilization in cement hydrate phases (compare Park et al., 2025).

The analysis of anions yields a similar behavior with variations between different concrete fines. After thermal activation, nitrite, nitrate, and sulfate content in the eluate decrease, while chloride and bromide are unaffected. The eluates from concrete contain lower amounts of anions, except for sulfate, which increases alongside the increased sulfate content in CEM I (compare Table 1).

Measurements of the total organic carbon (TOC) in unprocessed and processed concrete fines show an almost complete decomposition during thermal activation (Table 1). The same effect is apparent in the eluates, where the content of polycyclic aromatic hydrocarbons (PAH16) significantly reduces after thermal activation.

Ultimately, these results show that chrome, copper and sulfate are of special concern with regards to individual use cases. The exceedance of threshold concentrations (as defined through national regulations such as ErsatzbaustoffV (2021)) may preclude certain applications.

4. Conclusion

The substitution of Portland cement with waste materials impacts concrete compressive strength alongside other mechanical parameters and durability. This study compares the impact of granulated blast-furnace slag, fly ash, or limestone powder to six concrete fines of different origin and composition. For each supplementary cementitious material, the analysis uses a dual approach with the mitigation of compressive strength loss in contrast to an unaccounted substitution. This allows for the assessment of concrete performance at a constant compressive strength level.

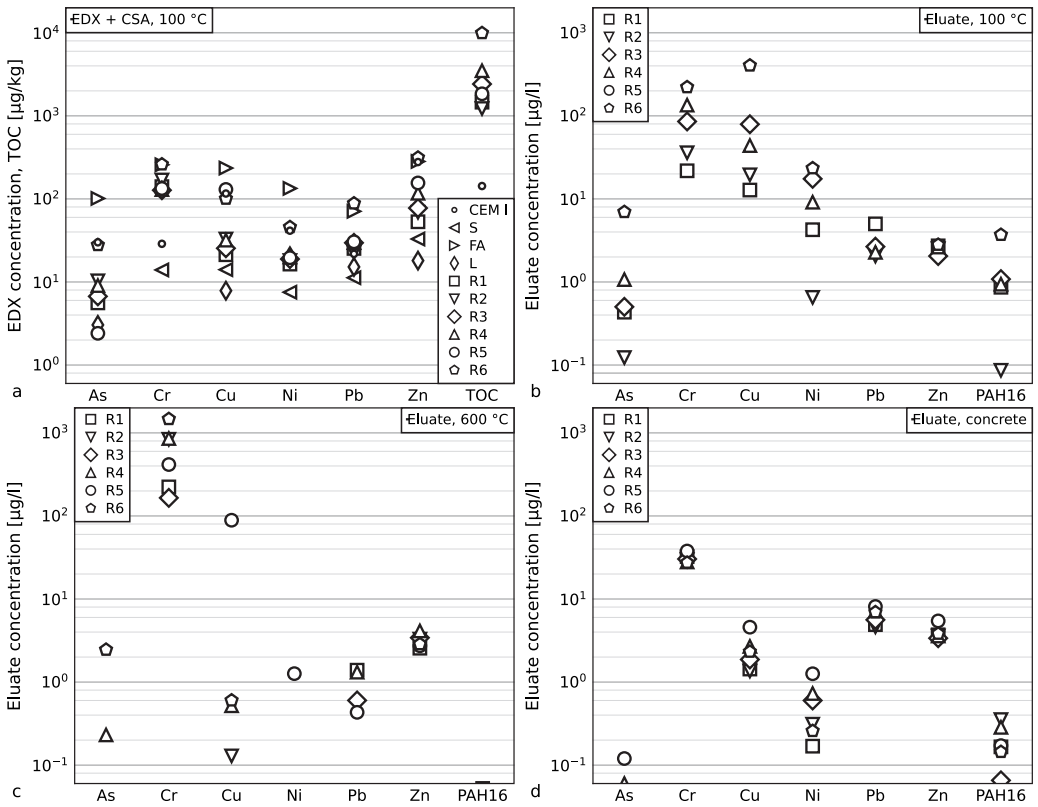

Fig. 10. Results of metal concentrations and total organic carbon content (TOC) and PAH16 concentrations. a: precursors through EDX and CSA, b: elutates from precursors ("100 °C"), c: thermally activated, unmilled concrete fines ("600 °C"), d: concrete mixes "–1" containing activated, milled concrete fines.

- Concrete containing thermally activated concrete fines or limestone powder exhibits a fast strength development, while fly ash or slag show a higher strength increase with later ages.
- Overall, flexural strength, the dynamic modulus of elasticity, and capillary water absorption are not affected beyond compressive strength reduction. A mitigation of strength loss also largely negates deviations in these concrete performance parameters.
- Concrete containing activated concrete fines exhibits higher shrinkage deformations compared to concrete with established SCMs.
- Chloride ingress and carbonation are increased for concrete containing activated fines compared to a CEM I-reference, but perform similarly to established SCMs. The only exception is the chloride binding capacity of hydration products from slag or fly ash, which is missing in activated fines.
- Concrete fines may contain harmful substances. The elution of those mostly reduces following thermal activation, with the notable exception of chrome.

In conclusion, the present results show a sufficient agreement of concrete with established SCMs and concrete containing thermally activated concrete fines of different origins. Therefore, a cement substitution of 30 wt% is feasible to obtain concrete mixtures, which agree with existing building standards and the underlying empirical relationships between compressive strength, mechanical properties, and durability. However, the simplifications chosen for enabling the qualitative comparison of a broad set of concrete properties require additional research. These procedures require a closer alignment with standardized experimental setups. Furthermore, the present results underline the need for investigating binding mechanisms of (re) activated cement hydrates and harmful substances, such as CO_2, chlorides, or heavy metals. A scaled-up industrial application of thermally activated concrete fines requires the quantitative assessment of harmful substance contents in the eluates with regard to threshold values defined for individual use cases.

CRediT authorship contribution statement

Jan P. Höffgen: Writing – original draft, Visualization, Methodology, Funding acquisition, Formal analysis, Conceptualization. **Lukas Reichert:** Writing – review & editing, Formal analysis. **Bernd Susset:** Writing – review & editing, Conceptualization. **Annegret Walz:** Writing – review & editing, Methodology, Formal analysis. **Peter Grathwohl:** Validation, Resources. **Frank Dehn:** Writing – review & editing, Supervision, Project administration, Funding acquisition.

Declaration of Generative AI and AI-assisted technologies in the writing process

During the preparation of this work, the authors used Grammarly and DeepL in order to check for spelling and wording errors. After using these tools/services, the authors reviewed and edited the content as needed and take full responsibility for the content of the published article.

Funding

This work was supported by the Dres. Edith und Klaus Dyckerhoff-Stiftung, grant no. T0218/36374.

Declaration of competing interest

The authors declare that they have no known competing financial interests or personal relationships that could have appeared to influence the work reported in this paper.

Appendix

See Tables A.2–A.6.

Data availability

Data will be made available on request.

Table A.2
Overview of different series. SCM: supplementary cementitious material. f: substitution rate of CEM I through SCM. k: assumed k-value. w/b: selected water-binder ratio. w/c_{eq}: resulting equivalent water–cement ratio. w: water content. c: CEM I content. a: SCM content. SP: superplasticizer dosage for achieving target consistency. Aggregate content for all series: RS: 526 kg/m³, RG: 1024 kg/m³.

Series	SCM	f –	k –	w/b –	w/c_{eq} –	w kg/m³	c kg/m³	a kg/m³	SP kg/m³
CEM I-1	CEM I	0.0		0.60	0.60	261	435		0.0
CEM I-2				0.50	0.50	244	488		0.0
S-1	S	0.3	0.8	0.50	0.53	242	339	145	0.0
S-2				0.46	0.49	234	356	153	0.0
FA-1	FA	0.3	0.5	0.50	0.61	233	327	140	0.0
FA-2				0.43	0.51	219	356	152	2.7
L-1	L	0.3	0.1	0.50	0.68	240	335	144	0.0
L-2				0.36	0.49	207	403	173	5.8
R1-1	R1-600	0.3	0.4	0.50	0.61	239	335	143	0.0
R1-2				0.40	0.49	217	380	163	5.6
R2-1	R2-600	0.3	0.4	0.50	0.61	239	334	143	0.0
R2-2				0.40	0.49	217	380	163	5.4
R3-1	R3-600	0.3	0.5	0.50	0.59	239	334	143	0.0
R3-2				0.42	0.49	222	370	158	4.0
R4-1	R4-600	0.3	0.5	0.50	0.59	238	334	143	0.0
R4-2				0.42	0.49	221	369	158	3.3
R5-1	R5-600	0.3	0.6	0.50	0.57	239	334	143	3.6
R5-2				0.43	0.49	224	365	156	6.7
R6-1	R6-600	0.3	0.6	0.50	0.57	239	335	143	1.6
R6-2				0.43	0.49	224	365	157	5.2

Table A.3
Chemical composition of CEM I, reference SCMs (S, FA, L) and concrete fines (R1–R6) before activation. Oxide phases of main elements through WDXRF, trace elements through EDXRF. Empty entries indicate results below the analytical limit of determination.

	CEM I	S	FA	L	R1	R2	R3	R4	R5	R6
WDXRF [wt%]										
LOI	2.7	−0.9	1.7	39.3	15.3	8.9	21.2	15.0	18.8	17.1
Na_2O	0.0	0.2	0.4		0.4	0.6	0.4	0.6	0.4	1.0
MgO	1.9	5.5	1.2	1.1	1.4	0.8	1.7	1.6	2.0	2.4
Al_2O_3	4.8	11.0	29.2	2.5	4.4	4.8	5.1	5.8	6.0	8.5
SiO_2	20.0	34.9	47.6	6.1	51.3	66.8	43.1	49.7	40.0	44.4
P_2O_5	0.2	0.0	0.3	0.0	0.1	0.1	0.1	0.1	0.1	0.2
K_2O	0.8	0.7	1.3	0.7	1.2	1.5	1.2	1.5	0.6	1.8
CaO	61.7	41.6	3.1	47.2	21.5	12.6	23.4	21.6	27.6	18.6
TiO_2	0.2	1.0	3.4	0.1	0.2	0.2	0.2	0.2	0.3	0.4
MnO	0.2	0.6	0.1	0.0	0.0	0.0	0.0	0.1	0.1	0.1
Fe_2O_3	3.1	1.2	9.0	0.9	1.7	1.6	2.1	2.4	1.7	4.2
EDXRF [mg/kg]										
As	30		101	3	6	10	7	9	2	28
Ba	520	1823	1097	99	310	289	530	322	347	377
Cd	0	0	1	0	1	1		1		
Cr	29	14	258		141	169	127	130	134	261
Cs	13	7	32	9	9		3	5		
Cu	116	14	235	8	21	33	25	32	130	101
Ga	11	8	47	10	11	11	11	11	10	14
Mo	4		9	1	3	5	4	4	3	7
Nb	6	4	126	4	7	6	7	7	7	13
Ni	41	8	134	20	16	18	19	20	20	46
Pb	22	11	71	15	25	23	30	30	30	88
Rb	35	23	117	26	49	63	47	56	25	93
Sb	21	12	6	4						
Sn	49	40	32	22	3	9	5	6	5	5
Sr	703	664	571	986	341	307	355	342	371	526
Th		10	27						3	3
U	1	10	11	5	0	1	1	1	2	1
V	60	62	393	49	45	41	45	50	57	66
Y	20	51	52	4	10	10	13	17	19	22
Zn	278	33	283	18	53	69	78	117	156	315
Zr	67	200	411	45	68	70	94	99	109	136

Table A.4
Results from the eluate analysis on unprocessed concrete fines ("−100"). n.d.: not determined, <l.o.d.: below the limit of detection. Note that, for R5-100, the automatic deactivation failed, resulting in an increase in W/S.

		R1-100	R2-100	R3-100	R4-100	R5-100	R6-100
Sample (dry)	g	669	740	545	465	247	394
Eluate	g	1339	1481	1085	914	1538	771
W/S	–	2.00	2.00	1.99	1.97	6.22	1.96
pH	–	12.50	12.15	12.25	12.15	12.38	10.03
Elect. conduct.	mS/cm	6.55	2.90	3.84	3.73	3.80	2.24
Fluoride	mg/l	n.d.	n.d.	n.d.	n.d.	n.d.	n.d.
Chloride	mg/l	82.59	10.36	118.44	26.69	18.64	118.05
Nitrite	mg/l	1.37	0.41	2.29	2.22	0.54	2.86
Bromide	mg/l	0.18	0.20	0.23	0.23	0.52	0.82
Nitrate	mg/l	10.82	1.67	9.35	9.58	1.01	23.20
Phosphate	mg/l	<l.o.d.	<l.o.d.	<l.o.d.	<l.o.d.	<l.o.d.	<l.o.d.
Sulfate	mg/l	33.86	15.61	26.57	391.31	35.44	1233.92
As	µg/l	0.43	0.12	0.50	1.07	0.03	6.97
Cd	µg/l	<l.o.d.	<l.o.d.	<l.o.d.	<l.o.d.	<l.o.d.	<l.o.d.
Cr	µg/l	21.82	35.98	85.67	134.84	77.88	221.85
Co	µg/l	0.43	5.54	10.91	1.92	0.76	18.66
Cu	µg/l	12.79	19.52	79.29	43.91	23.26	404.80
Ni	µg/l	4.26	0.65	17.46	9.13	1.63	23.44
Pb	µg/l	5.01	2.05	2.66	2.27	2.04	<l.o.d.
Th	µg/l	<l.o.d.	<l.o.d.	<l.o.d.	<l.o.d.	0.16	<l.o.d.
Zn	µg/l	2.72	2.52	2.05	2.63	3.54	2.81
PAH16	µg/l	0.86	0.09	1.08	0.94	0.35	3.70

Table A.5
Results from the eluate analysis on thermally activated concrete fines ("−600"). n.d.: not determined, <l.o.d.: below the limit of detection.

		R1-600	R2-600	R3-600	R4-600	R5-600	R6-600
Sample (dry)	g	132	136	97	90	131	70
Eluate	g	263	265	197	182	0	163
W/S	–	1.99	1.95	2.03	2.02	0.00	2.32
pH	–	12.26	12.16	12.15	12.23	12.09	10.57
Elect. conduct.	mS/cm	3.45	1.85	2.97	3.30	2.39	2.66
Fluoride	mg/l	0.88	0.65	0.94	1.28	0.67	n.d.
Chloride	mg/l	73.14	13.92	116.11	26.14	22.76	n.d.
Nitrite	mg/l	<l.o.d.	<l.o.d.	<l.o.d.	<l.o.d.	<l.o.d.	n.d.
Bromide	mg/l	0.24	0.24	0.31	0.30	0.15	n.d.
Nitrate	mg/l	<l.o.d.	<l.o.d.	<l.o.d.	<l.o.d.	<l.o.d.	n.d.
Phosphate	mg/l	<l.o.d.	<l.o.d.	<l.o.d.	<l.o.d.	<l.o.d.	n.d.
Sulfate	mg/l	7.60	21.66	8.65	25.48	25.99	n.d.
As	µg/l	<l.o.d.	<l.o.d.	<l.o.d.	0.23	<l.o.d.	2.45
Cd	µg/l	<l.o.d.	<l.o.d.	<l.o.d.	<l.o.d.	<l.o.d.	<l.o.d.
Cr	µg/l	223.80	838.77	165.17	856.13	416.18	1471.60
Co	µg/l	<l.o.d.	<l.o.d.	<l.o.d.	<l.o.d.	<l.o.d.	<l.o.d.
Cu	µg/l	<l.o.d.	0.13	<l.o.d.	0.52	88.87	0.60
Ni	µg/l	<l.o.d.	<l.o.d.	<l.o.d.	<l.o.d.	1.26	<l.o.d.
Pb	µg/l	1.39	<l.o.d.	0.60	1.32	0.43	<l.o.d.
Th	µg/l	<l.o.d.	<l.o.d.	<l.o.d.	<l.o.d.	<l.o.d.	0.03
Zn	µg/l	2.56	3.29	3.42	4.13	2.74	2.86
PAH16	µg/l	0.05	0.01	0.00	0.00	0.02	0.02

Table A.6
Results from the eluate analysis on concrete containing activated fines ("–1"). n.d.: not determined, <l.o.d.: below the limit of detection.

		R1-1	R2-1	R3-1	R4-1	R5-1	R6-1
Sample (dry)	g	656	683	657	650	636	700
Eluate	g	1313	1369	1329	1300	1278	1371
W/S	–	2.00	2.00	2.02	2.00	2.01	1.96
pH	–	12.60	12.60	12.69	12.63	12.77	12.70
Elect. conduct.	mS/cm	7.77	7.82	7.45	8.18	8.28	7.82

(*continued on next page*)

Table A.6 (*continued*).

		R1-1	R2-1	R3-1	R4-1	R5-1	R6-1
Fluoride	mg/l	n.d.	n.d.	n.d.	n.d.	n.d.	n.d.
Chloride	mg/l	45.35	28.74	38.87	32.91	38.03	29.77
Nitrite	mg/l	<l.o.d.	<l.o.d.	<l.o.d.	<l.o.d.	0.50	0.43
Bromide	mg/l	0.51	0.38	0.50	<l.o.d.	<l.o.d.	<l.o.d.
Nitrate	mg/l	1.71	1.66	1.60	1.95	8.77	3.93
Phosphate	mg/l	<l.o.d.	<l.o.d.	<l.o.d.	<l.o.d.	<l.o.d.	<l.o.d.
Sulfate	mg/l	71.55	53.07	74.29	48.63	74.73	47.54
As	µg/l	<l.o.d.	0.02	<l.o.d.	0.06	0.12	0.04
Cd	µg/l	<l.o.d.	<l.o.d.	<l.o.d.	<l.o.d.	<l.o.d.	<l.o.d.
Cr	µg/l	32.37	29.82	30.32	27.92	37.83	27.40
Co	µg/l	36.02	37.40	37.99	48.98	53.74	46.25
Cu	µg/l	1.44	1.36	1.87	2.69	4.58	2.32
Ni	µg/l	0.17	0.31	0.60	0.73	1.26	0.26
Pb	µg/l	4.91	4.63	5.62	7.16	8.13	6.95
Th	µg/l	<l.o.d.	<l.o.d.	<l.o.d.	<l.o.d.	0.00	<l.o.d.
Zn	µg/l	3.71	3.59	3.37	3.59	5.45	3.82
PAH16	µg/l	0.17	0.35	0.07	0.28	0.17	0.14

References

Algourdin, N., Nguyen, Q., Mesticou, Z., Si Larbi, A., 2021. Durability of recycled fine mortars under freeze–thaw cycles. Constr. Build. Mater. 291, 123330. http://dx.doi.org/10.1016/j.conbuildmat.2021.123330.

Amran, M., Murali, G., Khalid, N.H.A., Fediuk, R., Ozbakkaloglu, T., Lee, Y.H., Haruna, S., Lee, Y.Y., 2021. Slag uses in making an ecofriendly and sustainable concrete: A review. Constr. Build. Mater. 272, 121942. http://dx.doi.org/10.1016/j.conbuildmat.2020.121942.

Andrade, J.F.C., Córdoba, R.E., Schalch, V., 2025. Effect of presence of paint in recycled aggregates on the leaching of pollutants. Constr. Build. Mater. 485, 141904. http://dx.doi.org/10.1016/j.conbuildmat.2025.141904.

Andrade Neto, J., Carvalho, I., Monteiro, P., De Matos, P., Kirchheim, A., 2025. Unveiling the key factors for clinker reactivity and cement performance: A physic-chemical and performance investigation of 40 industrial clinkers. Cem. Concr. Res. 187, 107717. http://dx.doi.org/10.1016/j.cemconres.2024.107717.

Angulo, S.C., Guilge, M.S., Quarcioni, V.A., Cincotto, M.A., Nobre, T.R., Pöllmann, H., 2022. The role of calcium silicates and quicklime on the reactivity of rehydrated cements. Constr. Build. Mater. 340, 127625. http://dx.doi.org/10.1016/j.conbuildmat.2022.127625.

Aquino Rocha, J.H., Toledo Filho, R.D., 2023. The utilization of recycled concrete powder as supplementary cementitious material in cement-based materials: A systematic literature review. J. Build. Eng. 76, 107319. http://dx.doi.org/10.1016/j.jobe.2023.107319.

Baggio, T.F., Possan, E., De Oliveira Andrade, J.J., 2024. Physical-chemical characterization of construction and demolition waste powder with thermomechanical activation for use as supplementary cementitious material. Constr. Build. Mater. 437, 136907. http://dx.doi.org/10.1016/j.conbuildmat.2024.136907.

Baldusco, R., Nobre, T.R.S., Angulo, S.C., Quarcioni, V.A., Cincotto, M.A., 2019. Dehydration and rehydration of blast furnace slag cement. J. Mater. Civ. Eng. 31 (8), 04019132. http://dx.doi.org/10.1061/(ASCE)MT.1943-5533.0002725.

Baquerizo, L.G., Matschei, T., Scrivener, K.L., 2016. Impact of water activity on the stability of ettringite. Cem. Concr. Res. 79, 31–44. http://dx.doi.org/10.1016/j.cemconres.2015.07.008.

Barthel, M., Rübner, K., Kühne, H.-C., Rogge, A., Dehn, F., 2016. From waste materials to products for use in the cement industry. Adv. Cem. Res. 28 (7), 458–468. http://dx.doi.org/10.1680/jadcr.15.00149.

Bogas, J.A., Carriço, A., Pereira, M., 2019. Mechanical characterization of thermal activated low-carbon recycled cement mortars. J. Clean. Prod. 218, 377–389. http://dx.doi.org/10.1016/j.jclepro.2019.01.325.

Bogas, J.A., Carriço, A., Real, S., 2022a. Durability of concrete produced with recycled cement from waste concrete. Mater. Today: Proc. 58, 1149–1154. http://dx.doi.org/10.1016/j.matpr.2022.01.280.

Bogas, J.A., Carriço, A., Tenza-Abril, A.J., 2020. Microstructure of thermoactivated recycled cement pastes. Cem. Concr. Res. 138, 106226. http://dx.doi.org/10.1016/j.cemconres.2020.106226.

Bogas, J.A., Real, S., Carriço, A., Abrantes, J., Guedes, M., 2022b. Hydration and phase development of recycled cement. Cem. Concr. Compos. 127, 104405. http://dx.doi.org/10.1016/j.cemconcomp.2022.104405.

Campos, R., Larrain, M.M.M., Zaman, M., Pozadas, V., 2021. Relationships between compressive and flexural strengths of concrete based on fresh field properties. Int. J. Pavement Res. Technol. 14 (2), 161–167. http://dx.doi.org/10.1007/s42947-020-1074-0.

Carriço, A., Bogas, J.A., Guedes, M., 2020a. Thermoactivated cementitious materials – A review. Constr. Build. Mater. 250, 118873. http://dx.doi.org/10.1016/j.conbuildmat.2020.118873.

Carriço, A., Bogas, J.A., Hu, S., Real, S., Costa Pereira, M.F., 2021a. Novel separation process for obtaining recycled cement and high-quality recycled sand from waste hardened concrete. J. Clean. Prod. 309, 127375. http://dx.doi.org/10.1016/j.jclepro.2021.127375.

Carriço, A., Bogas, J.A., Real, S., Pereira, M.F.C., 2022. Shrinkage and sorptivity of mortars with thermoactivated recycled cement. Constr. Build. Mater. 333, 127392. http://dx.doi.org/10.1016/j.conbuildmat.2022.127392.

Carriço, A., Real, S., Bogas, J.A., 2021b. Durability performance of thermoactivated recycled cement concrete. Cem. Concr. Compos. 124, http://dx.doi.org/10.1016/j.cemconcomp.2021.104270.

Carriço, A., Real, S., Bogas, J.A., Costa Pereira, M.F., 2020b. Mortars with thermo activated recycled cement: Fresh and mechanical characterisation. Constr. Build. Mater. 256, 119502. http://dx.doi.org/10.1016/j.conbuildmat.2020.119502.

Chen, L., Wei, M., Lei, N., Li, H., 2024. Effect of chemical–thermal activation on the properties of recycled fine powder cementitious materials. Case Stud. Constr. Mater. 20, e02956. http://dx.doi.org/10.1016/j.cscm.2024.e02956.

Coffetti, D., Crotti, E., Gazzaniga, G., Carrara, M., Pastore, T., Coppola, L., 2022. Pathways towards sustainable concrete. Cem. Concr. Res. 154, 106718. http://dx.doi.org/10.1016/j.cemconres.2022.106718.

Darquennes, A., Rozière, E., Khokhar, M.I.A., Turcry, Ph., Loukili, A., Grondin, F., 2012. Long-term deformations and cracking risk of concrete with high content of mineral additions. Mater. Struct. 45 (11), 1705–1716. http://dx.doi.org/10.1617/s11527-012-9867-5.

Ekin, N., Uyanik, O., 2021. Comparison of static and dynamic elastic moduli in concrete: Effects of compressive strength, curing conditions and reinforcement. Iran. J. Sci. Technol. Trans. Civ. Eng. 45 (4), 2327–2343. http://dx.doi.org/10.1007/s40996-020-00513-7.

Engelsen, C.J., Van Der Sloot, H.A., Wibetoe, G., Justnes, H., Lund, W., Stoltenberg-Hansson, E., 2010. Leaching characterisation and geochemical modelling of minor and trace elements released from recycled concrete aggregates. Cem. Concr. Res. 40 (12), 1639–1649. http://dx.doi.org/10.1016/j.cemconres.2010.08.001.

ErsatzbaustoffV, 2021. Verordnung zur Einführung einer Ersatzbaustoffverordnung, zur Neufassung der Bundes-Bodenschutz- und Altlastenverordnung und zur Änderung der Deponieverordnung und der Gewerbeabfallverordnung: ErsatzbaustoffV.

Florea, M.V.A., 2014. Secondary Materials Applied in Cement-Based Products : Treatment, Modelling and Environmental Interaction (Ph.D. thesis). Technische Universiteit Eindhoven, http://dx.doi.org/10.6100/IR772902.

Friol Guedes de Paiva, F., Tamashiro, J.R., Pereira Silva, L.H., Kinoshita, A., 2021. Utilization of inorganic solid wastes in cementitious materials – A systematic literature review. Constr. Build. Mater. 285, 122833. http://dx.doi.org/10.1016/j.conbuildmat.2021.122833.

Gao, X., Gu, Y., Xie, T., Zhen, G., Huang, S., Zhao, Y., 2015. Characterization and environmental risk assessment of heavy metals in construction and demolition wastes from five sources (chemical, metallurgical and light industries, and residential and recycled aggregates). Environ. Sci. Pollut. Res. 22 (12), 9332–9344. http://dx.doi.org/10.1007/s11356-014-4058-2.

Gao, Y., Schutter, G., Ye, G., Yu, Z., Tan, Z., Wu, K., 2013. A microscopic study on ternary blended cement based composites. Constr. Build. Mater. 46, 28–38. http://dx.doi.org/10.1016/j.conbuildmat.2013.04.021.

Getachew, E.M., Yifru, B.W., Habtegebreal, B.T., Yehualaw, M.D., 2024. Performance evaluation of mortar with ground and thermo-activated recycled concrete cement. Cogent Eng. 11 (1), 2357726. http://dx.doi.org/10.1080/23311916.2024.2357726.

Gruyaert, E., Maes, M., De Belie, N., 2013a. Performance of BFS concrete: K-Value concept versus equivalent performance concept. Constr. Build. Mater. 47, 441–455. http://dx.doi.org/10.1016/j.conbuildmat.2013.05.006.

Gruyaert, E., Van Den Heede, P., De Belie, N., 2013b. Carbonation of slag concrete: Effect of the cement replacement level and curing on the carbonation coefficient – Effect of carbonation on the pore structure. Cem. Concr. Compos. 35 (1), 39–48. http://dx.doi.org/10.1016/j.cemconcomp.2012.08.024.

Güneyisi, E., Gesoğlu, M., 2008. A study on durability properties of high-performance concretes incorporating high replacement levels of slag. Mater. Struct. 41 (3), 479–493. http://dx.doi.org/10.1617/s11527-007-9260-y.

He, Z., Hu, R., Ma, Z., Liu, X., Wang, C., Wu, H., 2023. Reusing thermoactivated construction waste spoil as sustainable binder for durable concrete: Microstructure and chloride transport. Constr. Build. Mater. 398, 132553. http://dx.doi.org/10.1016/j.conbuildmat.2023.132553.

Herrmann, A., Koenig, A., Dehn, F., 2018. Structural concrete based on alkali-activated binders: Terminology, reaction mechanisms, mix designs and performance. Struct. Concr. 19 (3), 918–929. http://dx.doi.org/10.1002/suco.201700016.

Höffgen, J.P., Bruckschlögl, S., Wetz, B., Dehn, F., 2025. Influence of thermally activated industrial concrete fines of different origin on mortar strength development. Case Stud. Constr. Mater. e05427. http://dx.doi.org/10.1016/j.cscm.2025.e05427.

Höffgen, J.P., Dehn, F., 2025. Influence of thermally activated artificial concrete fines composition on mortar strength development. Dev. the Built Environ. 24, 100775. http://dx.doi.org/10.1016/j.dibe.2025.100775.

Höffgen, J.P., Schmitt, M., Dehn, F., 2026. Influence of thermally activated artificial concrete fines composition on concrete long-term behavior. J. Build. Eng. 112, 115767. http://dx.doi.org/10.1016/j.jobe.2026.115767.

Horváth, I., Proks, I., Nerád, I., 1977. Activation energies of the thermal decompositions of C3AH6 AND C3AD6 by the isothermal TG method. J. Therm. Anal. 12 (1), 105–110. http://dx.doi.org/10.1007/BF01909862.

International Federation for Structural Concrete (Ed.), 2023. Fib Model Code for Concrete Structures (2020), Version 1 International Federation for Structural Concrete (fib), Lausanne.

Juan, M.S., Gutiérrez, P.A., 2009. Study on the influence of attached mortar content on the properties of recycled concrete aggregate. Constr. Build. Mater. 23 (2), 872–877. http://dx.doi.org/10.1016/j.conbuildmat.2008.04.012.

Kalinowska-Wichrowska, K., Kosior-Kazberuk, M., Pawluczuk, E., 2020. The properties of composites with recycled cement mortar used as a supplementary cementitious material. Materials 13 (1), 64. http://dx.doi.org/10.3390/ma13010064.

Kaliyavaradhan, S.K., Ling, T.-C., Mo, K.H., 2020. Valorization of waste powders from cement-concrete life cycle: A pathway to circular future. J. Clean. Prod. 268, 122358. http://dx.doi.org/10.1016/j.jclepro.2020.122358.

Kim, J., Kim, N., 2023. Exploring the role of thermal activation of cement exposed to the external environment on the improvement of concrete properties. J. Mater. Res. Technol. 24, 2868–2878. http://dx.doi.org/10.1016/j.jmrt.2023.03.195.

Kim, J.-H., Seo, E.-A., Kim, D.-G., Chung, C.-W., 2021. Utilization of recycled cement powder as a solidifying agent for radioactive waste immobilization. Constr. Build. Mater. 289, 123126. http://dx.doi.org/10.1016/j.conbuildmat.2021.123126.

Kim, J., Ubysz, A., 2024. Thermal activation of multi-recycled concrete powder as supplementary cementitious material for repeated and waste-free recycling. J. Build. Eng. 98, 111169. http://dx.doi.org/10.1016/j.jobe.2024.111169.

Klingsch, E.W., 2014. Explosive Spalling of Concrete in Fire (Ph.D. thesis). ETH Zurich, Zürich, http://dx.doi.org/10.3929/ethz-a-010243000.

Knight, K.A., Cunningham, P.R., Miller, S.A., 2023. Optimizing supplementary cementitious material replacement to minimize the environmental impacts of concrete. Cem. Concr. Compos. 139, 105049. http://dx.doi.org/10.1016/j.cemconcomp.2023.105049.

Koenders, E., Weise, K., Mayer, M., Morina, N., 2025. Werkstoffe im Bauwesen: Einführung für Bauingenieure und Architekten. Springer Fachmedien Wiesbaden, Wiesbaden, http://dx.doi.org/10.1007/978-3-658-49382-0.

Kurda, R., Silvestre, J.D., De Brito, J., 2018. Toxicity and environmental and economic performance of fly ash and recycled concrete aggregates use in concrete: A review. Heliyon 4 (4), e00611. http://dx.doi.org/10.1016/j.heliyon.2018.e00611.

Lipowsky, A., Müller, A., 2017. Gesteinsmehl als Zuschlagstoffe in hydraulischen Bindemitteln. Aufbereitungs-Technik/Mineral Process. 58 (12), 52–64.

Liu, J.-C., Hossain, U., Xuan, D., Asad Ali, H., Ng, S.T., Ye, H., 2023. Mechanical and durability performance of sustainable concretes containing conventional and emerging supplementary cementitious materials. Dev. the Built Environ. 15, 100197. http://dx.doi.org/10.1016/j.dibe.2023.100197.

Lu, C.-C., Hsu, M.H., Lin, Y.-P., 2019. Evaluation of heavy metal leachability of incinerating recycled aggregate and solidification/stabilization products for construction reuse using TCLP, multi-final pH and EDTA-mediated TCLP leaching tests. J. Hazard. Mater. 368, 336–344. http://dx.doi.org/10.1016/j.jhazmat.2019.01.066.

Lübeck, A., Gastaldini, A., Barin, D., Siqueira, H., 2012. Compressive strength and electrical properties of concrete with white Portland cement and blast-furnace slag. Cem. Concr. Compos. 34 (3), 392–399. http://dx.doi.org/10.1016/j.cemconcomp.2011.11.017.

Ma, X., He, T., Da, Y., Lin, Y., Feng, Y., Zhang, W., 2023. Evaluation of the ability of cement prepared with incineration fly ash to solidify heavy metals at high temperatures. J. Build. Eng. 78, 107559. http://dx.doi.org/10.1016/j.jobe.2023.107559.

Ma, Z., Shen, J., Wu, H., Zhang, P., 2022. Properties and activation modification of eco-friendly cementitious materials incorporating high-volume hydrated cement powder from construction waste. Constr. Build. Mater. 316, 125788. http://dx.doi.org/10.1016/j.conbuildmat.2021.125788.

Mao, Y., Hu, X., Alengaram, U.J., Chen, W., Shi, C., 2024. Use of carbonated recycled cement paste powder as a new supplementary cementitious material: A critical review. Cem. Concr. Compos. 154, 105783. http://dx.doi.org/10.1016/j.cemconcomp.2024.105783.

Marques, A.I., Morais, J., Morais, P., Veiga, M.D.R., Santos, C., Candeias, P., Ferreira, J.G., 2020. Modulus of elasticity of mortars: Static and dynamic analyses. Constr. Build. Mater. 232, 117216. http://dx.doi.org/10.1016/j.conbuildmat.2019.117216.

Müller, H.S., Acosta Urrea, F., Kvitsel, V., 2021. Modelle zur Vorhersage des Schwindens und Kriechens von Beton: Teil 1: Analyse des Schwindmodells in DIN EN 1992-1-1:2011 und neuer Ansatz im Eurocode 2 prEN 1992-1-1:2020. Beton- Und Stahlbetonbau 116 (1), 2–18. http://dx.doi.org/10.1002/best.202000082.

Nath, P., Sarker, P., 2011. Effect of fly ash on the durability properties of high strength concrete. Procedia Eng. 14, 1149–1156. http://dx.doi.org/10.1016/j.proeng.2011.07.144.

Noel, N., Mielke, T., Semugaza, G., Gierth, A.Z., Helmich, S., Nawrath, S., Lupascu, D.C., 2025. Chemical transformations during the preparation and rehydration of reactivated virgin cements. Cement 19, 100129. http://dx.doi.org/10.1016/j.cement.2025.100129.

Ohemeng, E.A., Ekolu, S.O., 2020. A review on the reactivation of hardened cement paste and treatment of recycled aggregates. Mag. Concr. Res. 72 (10), 526–539. http://dx.doi.org/10.1680/jmacr.18.00452.

Orozco, C., Babel, S., Tangtermsirikul, S., Sugiyama, T., 2024. Comparison of environmental impacts of fly ash and slag as cement replacement materials for mass concrete and the impact of transportation. Sustain. Mater. Technol. 39, e00796. http://dx.doi.org/10.1016/j.susmat.2023.e00796.

Panesar, D.K., Zhang, R., 2020. Performance comparison of cement replacing materials in concrete: Limestone fillers and supplementary cementing materials – A review. Constr. Build. Mater. 251, 118866. http://dx.doi.org/10.1016/j.conbuildmat.2020.118866.

Park, K.S., Zajac, M., Matschei, T., Vollpracht, A., 2025. The fate of heavy metals in recycled concrete paste upon enforced carbonation: A review. Resour. Conserv. Recycl. Adv. 28, 200289. http://dx.doi.org/10.1016/j.rcradv.2025.200289.

Pavlů, T., 2018. The utilization of recycled materials for concrete and cement production- A review. IOP Conf. Ser.: Mater. Sci. Eng. 442 (1), 012014. http://dx.doi.org/10.1088/1757-899X/442/1/012014.

Qian, D., Yu, R., Shui, Z., Sun, Y., Jiang, C., Zhou, F., Ding, M., Tong, X., He, Y., 2020. A novel development of green ultra-high performance concrete (UHPC) based on appropriate application of recycled cementitious material. J. Clean. Prod. 261, 121231. http://dx.doi.org/10.1016/j.jclepro.2020.121231.

Rakhimova, N., Shi, C., 2024. Upcycling of concrete wastes as precursors in alkali-activated materials: A review. Constr. Build. Mater. 436, 136978. http://dx.doi.org/10.1016/j.conbuildmat.2024.136978.

Real, S., Bogas, J.A., Carriço, A., Hu, S., 2021. Mechanical characterisation and shrinkage of thermoactivated recycled cement concrete. Appl. Sci. 11 (6), 2454. http://dx.doi.org/10.3390/app11062454.

Real, S., Carriço, A., Bogas, J.A., Guedes, M., 2020. Influence of the treatment temperature on the microstructure and hydration behavior of thermoactivated recycled cement. Materials 13 (18), 3937. http://dx.doi.org/10.3390/ma13183937.

Sakthivel, T., Gettu, R., Pillai, R.G., 2019. Compressive strength and elastic modulus of concretes with fly ash and slag. J. Inst. Eng. (India): Ser. A 100 (4), 575–584. http://dx.doi.org/10.1007/s40030-019-00376-w.

Schneider, U., 1982. Verhalten von Beton Bei Hohen Temperaturen. DAfStb-Heft, vol. 337, Wilhelm Ernst und Sohn, Berlin.

Scrivener, K.L., Juilland, P., Monteiro, P.J., 2015. Advances in understanding hydration of Portland cement. Cem. Concr. Res. 78, 38–56. http://dx.doi.org/10.1016/j.cemconres.2015.05.025.

Semugaza, G., Mielke, T., Castillo, M.E., Gierth, A.Z., Tam, J.X., Nawrath, S., Lupascu, D.C., 2023. Reactivation of hydrated cement powder by thermal treatment for partial replacement of ordinary portland cement. Mater. Struct. 56 (3), http://dx.doi.org/10.1617/s11527-023-02133-9.

Serpell, R., Lopez, M., 2015. Properties of mortars produced with reactivated cementitious materials. Cem. Concr. Compos. 64, 16–26. http://dx.doi.org/10.1016/j.cemconcomp.2015.08.003.

Snellings, R., Suraneni, P., Skibsted, J., 2023. Future and emerging supplementary cementitious materials. Cem. Concr. Res. 171, 107199. http://dx.doi.org/10.1016/j.cemconres.2023.107199.

Sui, Y., Ou, C., Liu, S., Zhang, J., Tian, Q., 2020. Study on properties of waste concrete powder by thermal treatment and application in mortar. Appl. Sci. 10 (3), 998. http://dx.doi.org/10.3390/app10030998.

Tokareva, A., Kaassamani, S., Waldmann, D., 2023. Fine demolition wastes as Supplementary cementitious materials for CO2 reduced cement production. Constr. Build. Mater. 392, 131991. http://dx.doi.org/10.1016/j.conbuildmat.2023.131991.

Tokareva, A., Waldmann, D., 2025. Durability of cement mortars containing fine demolition wastes as supplementary cementitious materials. Constr. Build. Mater. 477, 141316. http://dx.doi.org/10.1016/j.conbuildmat.2025.141316.

Van Praagh, M., Modin, H., Trygg, J., 2015. Organic compounds in concrete from demolition works. Waste Manage. 45, 186–193. http://dx.doi.org/10.1016/j.wasman.2015.06.037.

Vashistha, P., Oinam, Y., Kim, H.-K., Pyo, S., 2023. Effect of thermo-mechanical activation of waste concrete powder (WCP) on the characteristics of cement mixtures. Constr. Build. Mater. 362, 129713. http://dx.doi.org/10.1016/j.conbuildmat.2022.129713.

Vyšvařil, M., Bayer, P., Chromá, M., Rovnaníková, P., 2014. Physico-mechanical and microstructural properties of rehydrated blended cement pastes. Constr. Build. Mater. 54, 413–420. http://dx.doi.org/10.1016/j.conbuildmat.2013.12.021.

Wang, C.-q., Cheng, L.-x., Huang, Q.-c., Shui, Z.-h., Liu, Y.-y., Zhao, H., Zhang, Z.-j., 2023. Basic performance, heavy metal leaching mechanism and risk assessment analysis of waste concrete. Arch. Civ. Mech. Eng. 23 (2), 122. http://dx.doi.org/10.1007/s43452-023-00666-y.

Wang, J., Lacarrière, L., Sellier, A., 2019. Multicomponent modelling of cement paste dehydration under different heating rates. Mater. Struct. 52 (1), 6. http://dx.doi.org/10.1617/s11527-018-1306-9.

Wang, D., Shi, C., Farzadnia, N., Shi, Z., Jia, H., 2018. A review on effects of limestone powder on the properties of concrete. Constr. Build. Mater. 192, 153–166. http://dx.doi.org/10.1016/j.conbuildmat.2018.10.119.

Wang, S., Yu, H., Liu, S., Yaras, A., Hu, L., Zhang, W., Peng, M., Enkhchimeg, B., Mao, L., 2025. New insights into the environmental safety of incorporating Cr(III) into cement matrix: Cr(VI) formation driven by low-intensity fire. Constr. Build. Mater. 489, 140694. http://dx.doi.org/10.1016/j.conbuildmat.2025.140694.

Wang, L., Yu, Z., Liu, B., Zhao, F., Tang, S., Jin, M., 2022. Effects of fly ash dosage on shrinkage, crack resistance and fractal characteristics of face slab concrete. Fractal Fract. 6 (6), 335. http://dx.doi.org/10.3390/fractalfract6060335.

Wei, M., Chen, L., Lei, N., Li, H., Huang, L., 2024. Experimental investigation on freeze–thaw resistance of thermally activated recycled fine powder concrete. Constr. Build. Mater. 457, 139378. http://dx.doi.org/10.1016/j.conbuildmat.2024.139378.

Wei, M., Chen, L., Lei, N., Li, H., Huang, L., 2025. Mechanical properties and microstructures of thermally activated ultrafine recycled fine powder cementitious materials. Constr. Build. Mater. 475, 141195. http://dx.doi.org/10.1016/j.conbuildmat.2025.141195.

Weimann, K., 2009. Untersuchungen zur Nassaufbereitung von Betonbrechsand unter Verwendung der Setzmaschinentechnik. BAM-Dissertationsreihe, Bundesanstalt für Materialforschung und -prüfung (BAM), Berlin, no. 51.

Wu, H., Liang, C., Zhang, Z., Yao, P., Wang, C., Ma, Z., 2023. Utilizing heat treatment for making low-quality recycled aggregate into enhanced recycled aggregate, recycled cement and their fully recycled concrete. Constr. Build. Mater. 394, 132126. http://dx.doi.org/10.1016/j.conbuildmat.2023.132126.

Wu, H., Yang, D., Ma, Z., 2021. Micro-structure, mechanical and transport properties of cementitious materials with high-volume waste concrete powder and thermal modification. Constr. Build. Mater. 313, 125477. http://dx.doi.org/10.1016/j.conbuildmat.2021.125477.

Xi, X., Zheng, Y., Du, C., Zhang, P., Sun, M., 2024. Study on the hydration characteristics, mechanical properties, and microstructure of thermally activated low-carbon recycled cement. Constr. Build. Mater. 447, 138042. http://dx.doi.org/10.1016/j.conbuildmat.2024.138042.

Xu, L., Wang, J., Hu, X., Ran, B., Wu, T., Zhou, X., Xiong, Y., 2024. Physical performance, durability, and carbon emissions of recycled cement concrete and fully recycled concrete. Constr. Build. Mater. 447, 138128. http://dx.doi.org/10.1016/j.conbuildmat.2024.138128.

Xu, L., Wang, J., Li, K., Hao, T., Li, Z., Li, L., Ran, B., Du, H., 2023. New insights on dehydration at elevated temperature and rehydration of GGBS blended cement. Cem. Concr. Compos. 139, 105068. http://dx.doi.org/10.1016/j.cemconcomp.2023.105068.

Xu, L., Wang, J., Li, K., Lin, S., Li, M., Hao, T., Ling, Z., Xiang, D., Wang, T., 2022. A systematic review of factors affecting properties of thermal-activated recycled cement. Resour. Conserv. Recycl. 185, 106432. http://dx.doi.org/10.1016/j.resconrec.2022.106432.

Younsi, A., Turcry, P., Rozière, E., Aït-Mokhtar, A., Loukili, A., 2011. Performance-based design and carbonation of concrete with high fly ash content. Cem. Concr. Compos. 33 (10), 993–1000. http://dx.doi.org/10.1016/j.cemconcomp.2011.07.005.

Zelic, J., Ugrina, L., Jozic, D., 2007. Application of thermal methods in the chemistry of cement: Kinetic analysis of portlandite from non-isothermal thermogravimetric data. In: The First International Proficiency Testing Conference. n. d., Sinaia, Romania, pp. 420–429.

Zhang, D., Zhang, S., Huang, B., Yang, Q., Li, J., 2022. Comparison of mechanical, chemical, and thermal activation methods on the utilisation of recycled concrete powder from construction and demolition waste. J. Build. Eng. 61, 105295. http://dx.doi.org/10.1016/j.jobe.2022.105295.

Zheng, Y., Xi, X., Liu, H., Du, C., Lu, H., 2024. A review: Enhanced performance of recycled cement and CO2 emission reduction effects through thermal activation and nanosilica incorporation. Constr. Build. Mater. 422, 135763. http://dx.doi.org/10.1016/j.conbuildmat.2024.135763.

Zhou, Q., Glasser, F.P., 2001. Thermal stability and decomposition mechanisms of ettringite at <120°C. Cem. Concr. Res. 31 (9), 1333–1339. http://dx.doi.org/10.1016/S0008-8846(01)00558-0.

Zhou, Q., Lachowski, E.E., Glasser, F.P., 2004. Metaettringite, a decomposition product of ettringite. Cem. Concr. Res. 34 (4), 703–710. http://dx.doi.org/10.1016/j.cemconres.2003.10.027.